DC4GS: Directional Consistency-Driven Adaptive Density Control for 3D Gaussian Splatting

Moonsoo Jeong[1] **Dongbeen Kim**[2] **Minseong Kim**[3] **Sungkil Lee**[1,2,3,*]
[1]Department of Electrical and Computer Engineering, Sungkyunkwan University, South Korea
[2]Department of Computer Science and Engineering, Sungkyunkwan University, South Korea
[3]Department of Immersive Media Engineering, Sungkyunkwan University, South Korea
{moonsoo101, rlaehdqls021, leon0106, sungkil}@skku.edu

Abstract

We present a Directional Consistency (DC)-driven Adaptive Density Control (ADC) for 3D Gaussian Splatting (DC4GS). Whereas the conventional ADC bases its primitive splitting on the magnitudes of positional gradients, we further incorporate the DC of the gradients into ADC, and realize it through the angular coherence of the gradients. Our DC better captures local structural complexities in ADC, avoiding redundant splitting. When splitting is required, we again utilize the DC to define optimal split positions so that sub-primitives best align with the local structures than the conventional random placement. As a consequence, our DC4GS greatly reduces the number of primitives (up to 30% in our experiments) than the existing ADC, and also enhances reconstruction fidelity greatly.

1 Introduction

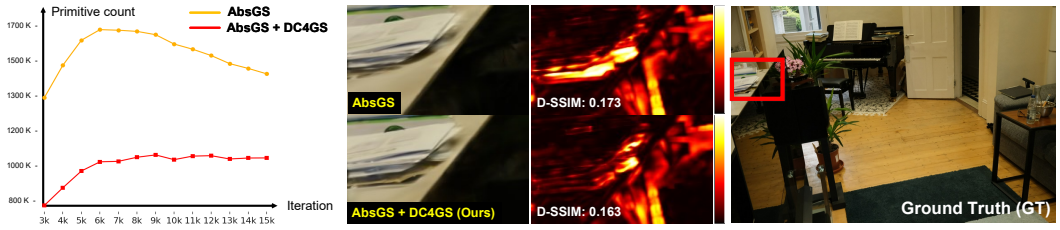

(a) Evolution of primitive counts during training (b) Rendering quality improvement in high-frequency details

Figure 1: Comparison of AbsGS [38] and our Directional Consistency-driven density control (DC4GS) in terms of (a) primitive counts during training and (b) reconstruction quality. DC4GS saturates much earlier (here, 6k iterations) than the AbsGS does. Upon convergence, it achieves a significant reduction in primitive counts (here, 30%) and high-quality splits as well, resulting in much higher reconstruction quality (b) for high-frequency details (here, see the red inset).

3D Gaussian Splatting (3DGS) can synthesize high-quality renderings well, even from *sparse* point clouds [14]. Its efficiency stems from its adaptive density control (ADC) that leverages 2D positional gradients, derived from reconstruction loss, indicating how effectively the observations of the input signals are represented. When the primitives in fact are likely to require finer details (i.e., over-reconstruction), the ADC spawns new primitives by splitting coarse ones where they matter most.

*Corresponding author.
Code is available at https://github.com/cgskku/dc4gs.

39th Conference on Neural Information Processing Systems (NeurIPS 2025).

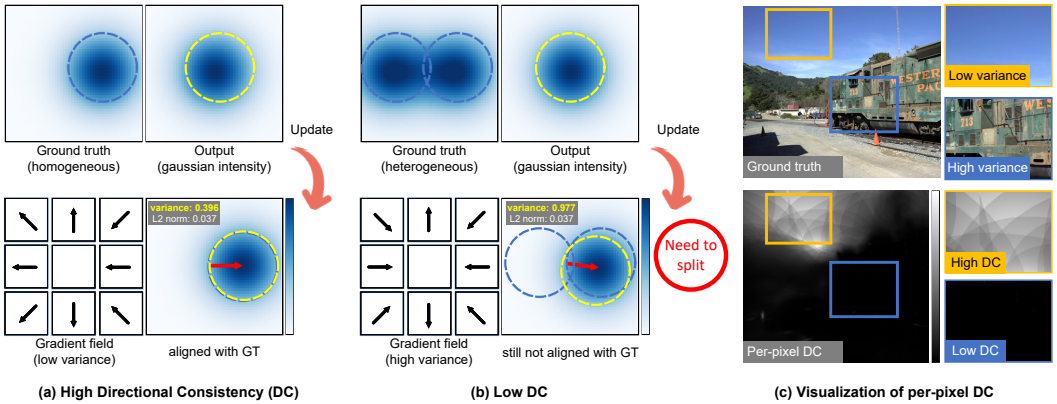

Figure 2: Visualization of how DC reflects structural complexities. In (a), a Gaussian can be aligned with a single-peak ground truth (GT) using a simple shift, which is indicated by a low angular variance (i.e., high DC). In contrast, (b) requires splitting due to the mismatch from the two-peak GT. This can be reflected in its divergent gradients (i.e., low DC), but not in the gradient magnitudes. (c) visualizes the per-pixel DC values in a real-world image, distinguishing directionally coherent (e.g., the sky) and incoherent (the train) regions well.

The positional gradients include valuable information of reconstruction, but the majority of the existing 3DGS-based methods still take only their magnitude (L2 norm) into account [14, 38, 40, 41, 44]. The amount of information available from the magnitude is limited in representing the distributions of individual primitives, and often leads to redundant splits where they are actually not required (e.g., low-frequency or already well-refined areas). Furthermore, split positions are randomly chosen and thereby disregard local structural cues, which often result in misaligned or overlapping sub-primitives.

In order for ADC to better reflect the homogeneity of the local structures, we exploit the directional distributions of the positional gradients as well as their magnitudes. When the directions of the gradients are coherent, the regions encompassing them are likely to be simpler, not requiring splitting. In contrast, regions with incoherent gradients require improving details. This approach can take advantages both of primitive counts and reconstruction quality (see Fig. 1 for example). To this end, we introduce *Directional Consistency* (DC) that captures the spatial coherence of the directional patterns of positional gradients within Gaussians. For its simple yet effective realization, our implementation uses the angular variance of gradient directions across pixels. Fig. 2 exemplifies the two Gaussian patterns whose gradient magnitudes are identical, but their DCs are different.

Building on this insight, we use DC as a versatile criterion in determining whether to split a primitive and where to place its sub-primitives. To guide the splitting, we incorporate DC into the existing ADC criteria, which better detects primitives in structurally complex regions. For split placement, we present a DC-guided split, splitting a primitive where the DCs of its sub-primitive candidates are maximized and the structural complexity each sub-primitive represents is minimized. By leveraging the DC cue in both decision and placement of splitting, we achieve higher reconstruction fidelity with much fewer primitives than the previous simpler approaches.

To summarize, the contributions of this paper can be listed in what follows:

- introduction of *Directional Consistency* (DC) as a criterion to better capture the structural complexity of local positional gradients in 3DGS;
- a DC-guided split decision so that structurally complex regions are better selected;
- a DC-guided split scheme so that the DCs of resulting sub-primitives are maximized and thereby their structures are best distinguished.

2 Related work

2.1 3D Gaussian splatting

The 3DGS [14] has emerged as a real-time alternative to Neural Radiance Fields (NeRFs) [24] that remains computationally intensive despite extensive advances in acceleration [5, 6, 9, 25, 28, 33, 39], anti-aliasing [1–3], and robustness [17, 34]. Unlike NeRFs, 3DGS enables efficient rendering by directly rasterizing explicit 3D Gaussian primitives without requiring dense regular grids/fields. However, 3DGS suffers from aliasing, blurring, and high-frequency detail loss in reconstruction [7].

To address aliasing from mismatched scale and insufficient filtering, several 3DGS-based methods [19, 21, 32, 40] introduce multiscale filtering and analytic rasterization to reduce artifacts and improve sharpness.

To better preserve high-frequency details and mitigate blurring caused by over-reconstruction, FreGS [42] applies progressive Fourier-space regularization to emphasize texture-rich structures, and BAGS [26] learns spatial blur kernels to recover over-smoothed details.

Geometric inconsistencies in 3DGS have also been addressed. Optimal-GS [13] reduces projection errors through local affine approximations, and Scaffold-GS [22] adopts anchor-based hierarchical representations, where neural anchors spawn offset primitives to model local structures, preserving global structural coherence.

2.2 Adaptive density control for 3D Gaussian splatting

The conventional ADC scheme in the 3DGS refines Gaussian primitives by iteratively splitting or cloning them based on positional gradient magnitudes. However, the ADC is sensitive to hyperparameters and often causes redundant splits and spatial misalignment.

To improve the selectivity of the ADC, several methods refine the processing of view-space positional gradients. AbsGS [38] and GOF [41] mitigate gradient cancellation by using the magnitude of homodirectional (absolute) gradients and the norm of positional gradients. Pixel-GS [44] introduces pixel-aware gradients by weighting contributions based on pixel coverage and view-space depth, densifying under-sampled regions.

The ADC was reformulated from alternative optimization perspectives. Revising Densification [29] guides growth via pixel-level error propagation, while a Markov Chain Monte Carlo-based method [15] interprets the ADC as stochastic sampling using Stochastic Gradient Langevin Dynamics [4] to reallocate inactive Gaussians without explicit densification.

Memory-efficient ADC is explored in Compact-3DGS [18], which prunes primitives using volume masks, and GES [10], which applies frequency-based pruning via generalized exponents. Recently, Localized Points Management (LPM) [37] improves ADC by identifying error-contributing zones under multi-view constraints and applying localized densification with opacity reset.

While the existing 3DGS-based methods often over-refine homogeneous regions and misalign sub-primitives, our work incorporates the DC to evaluate the homogeneity of Gaussians, enabling more selective splitting and better alignment with scene structure. This results in significant improvements in both the quality and storage efficiency.

3 Preliminary: adaptive density control in 3D Gaussian splatting

In this section, we briefly review the ADC in the standard 3DGS [14]. The 3DGS is typically initialized with sparse points derived from Structure-from-Motion (SfM) [30, 31], and densifies Gaussians via the ADC. This process entails evaluating view-space positional gradients $\partial L/\partial \mu'$, where L is reconstruction loss and μ' is the center of a projected 2D Gaussian. The gradients are used to identify regions requiring higher details. The ADC criterion $\nabla_{\mu'} L$ is computed every hundred optimization iterations, and is defined as the average magnitude of the positional gradients:

$$\nabla_{\mu'_i} L = \frac{1}{\nu} \sum_{v=1}^{\nu} \| \frac{\partial L_v}{\partial \mu'_{i,v}} \|, \tag{1}$$

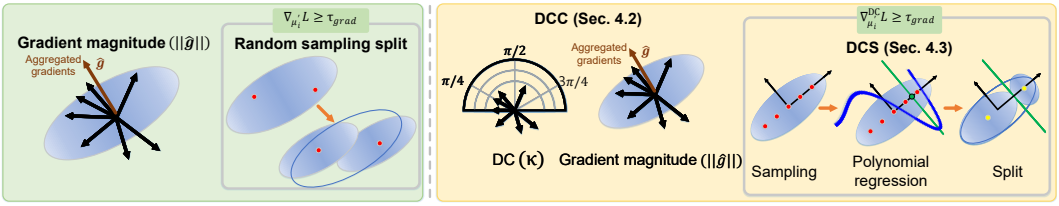

(a) Conventional ADC (b) DC4GS

Figure 3: Comparison of the conventional ADC scheme (e.g., 3DGS [14], AbsGS [38], and Pixel-GS [44]) and our DC4GS. (a) Gaussian primitives are selected using the positional gradient magnitude-based criterion, and the new Gaussians are randomly spawned within the pre-split Gaussian. (b) Our DC-based split Criterion (DCC) further integrates the DC (the circular mean of the positional gradients) into the previous ADC criterion. Also, our DC-guided Split (DCS) better places the new sub-primitives so that their DCs are best distinguished.

where ν denotes the number of views in which a Gaussian i is observed, and L_v is the loss for the view v. When $\nabla_{\mu_i'} L$ of a Gaussian exceeds a threshold τ_p and its maximum scale $\|S_i\|$ surpasses τ_S, the Gaussian i is split, and produces N sub-primitives (N=2 by default) by randomly sampling new centers within its coverage. If the gradient exceeds τ_p, but $\|S_i\|$ is below τ_S, the Gaussian is cloned in place. Gaussians with opacity below a given threshold are pruned out for efficiency.

We can extend not only the ADC criterion of the 3DGS in Eq. (1), but also the recent criteria still based on the gradient magnitude [38, 44], by incorporating DC into them. These extended criteria guide both the split decisions and sub-primitive placements. The details of how to define and apply our DC into the ADC are presented in Sec. 4.

4 DC4GS: Directional consistency-driven adaptive density control for 3DGS

The key idea of DC4GS is to quantify the directional coherence of positional gradients within a Gaussian primitive, which thereby enhances the gradient magnitude-based ADC schemes. The DC serves as an effective cue for assessing how homogeneous the region represented by a primitive is. We incorporate the DC into ADC to facilitate two key operations: 1) deciding whether a primitive should be split; 2) determining where to place sub-primitives when splitting is required.

To this end, we extend the existing densification criterion (Eq. (1)) by weighting it with the DC, which we refer to as the *DC-weighted split Criterion (DCC)*. When a DCC value is high, a single Gaussian primitive is likely to cover a heterogeneous region, which cannot adequately capture the region; this suggests refinement through splitting. Once a primitive is determined to be split, we also improve the placement of the newly spawned primitives; the conventional scheme places them randomly. We evaluate multiple candidate split locations within it and select the one that minimizes a DC-based cost. This divides a heterogeneous region into distinct sub-regions that are internally homogeneous. We referred this scheme as the *DC-guided Split (DCS)*.

Fig. 3 illustrates the differences between the conventional ADC and our DC4GS. Our DC4GS is readily compatible with the existing 3DGS-based pipelines, and thereby, can be easily plugged into their pipelines.

4.1 Directional consistency

The DC is computed from the positional gradients within a Gaussian, derived from reconstruction loss. Since the positional gradient magnitude also reflects how sensitive the loss is to positional changes, combining them together allows the 3DGS to better understand whether each primitive represents the regions well or not.

To quantify the DC within a Gaussian, we first assess the directional coherence of its positional gradients using a *circular mean* (or negative *circular variance*) [23] that is a statistical measure of angular dispersion of a set of unit vectors. Given a set of N unit vectors u_j, its circular mean is defined as $C = \frac{1}{N}\sum_{j=1}^{N} u_j$, and its L2 norm $\|C\|$ reflects directional alignment. $\|C\| \approx 1$ implies

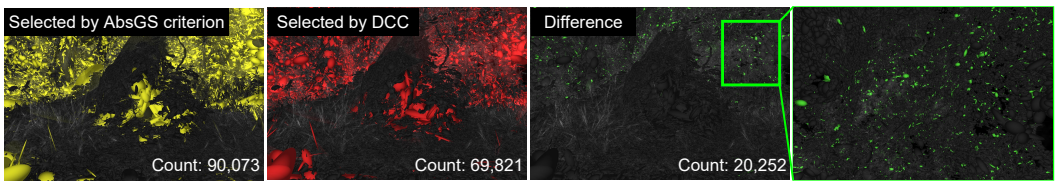

Figure 4: Comparison of split candidates selected by the criterion of AbsGS and DCC from the identical training states. After 14,900 training steps on the Stump scene using the 3DGS, Gaussians selected for splitting are visualized in yellow (AbsGS) and red (DCC). The difference (green) shows (potentially redundant) 20,252 Gaussians are not split by the DCC. Most of these differences are already of tiny sizes, suggesting limited structural gain from further splitting.

the vectors are aligned, and $\|C\| \approx 0$ implies angularly dispersed vectors. On the other hand, the circular variance is given by $V = 1 - \|C\| \in [0, 1]$, and represents directional inconsistency.

In our case, given a Gaussian i, we define its *directional consistency* $\kappa_i = \|C_i\|$. In the context of 3DGS, we evaluate the circular mean with respect to its positional gradients. For each pixel j influenced by the Gaussian i, let $g_{i,j} = \partial L_j / \partial {\mu'}_i$ be the positional gradient and $u_{i,j} = g_{i,j} / \|g_{i,j}\|$ be its unit vector. The circular mean C_i of the positional gradients is computed as:

$$C_i = \frac{1}{N} \sum_{j=1}^{N} u_{i,j} \in \mathbb{R}^2. \tag{2}$$

4.2 Directional consistency-weighted split criterion

Our DC can guide whether a Gaussian should be split. To this end, we introduce DC-guided split Criterion (DCC), which integrates the DC with the positional gradient magnitude. It identifies primitives that have a higher impact on the reconstruction and cover regions that cannot be well modeled by a single Gaussian.

To utilize DCC, we first aggregate the positional gradient magnitudes at pixels affected by Gaussian i as $\hat{g}_i = \sum_j |g_{i,j}|$, following the homodirectional positional gradients accumulation in AbsGS [38]. We use this formulation by default, but $\hat{g}_i$ can be replaced with other alternatives, such as that used in 3DGS (Eq. (1)) or Pixel-GS [44]; we demonstrate their integrations in Sec. 6.

Then, the DCC for Gaussian i can be defined as:

$$\nabla^{\mathrm{DC}}_{{\mu'}_i} L = \frac{1}{\nu} \sum_{v=1}^{\nu} (1 - \kappa_{i,v}) \cdot \|\hat{g}_{i,v}\|, \tag{3}$$

where ν is the number of views in which the Gaussian is visible, and $\kappa_{i,v}$ denotes the DC evaluated for view v. We follow the per-view averaging scheme of the 3DGS [14], but augment the positional gradient magnitude with the complement of the DC, $1 - \kappa_{i,v}$, as a weighting factor. The Gaussian i is selected for splitting, if its DCC, $\nabla^{\mathrm{DC}}_{{\mu'}_i} L$, exceeds the gradient threshold τ_p, and its maximum scale $\|S_i\|$ is smaller than the scale threshold τ_S. Gaussians with high DC values, typically corresponding to homogeneous regions, are thus excluded from splitting.

As shown in Fig. 4, DCC well filters out refined primitives that are unlikely to benefit from a succeeding subdivision, and thereby, reduces the effective number of primitives selected for splitting compared to the gradient magnitude-based criterion.

4.3 Directional consistency-guided split

Our DCS improves the previous random sub-primitive placement by selecting split locations so that each sub-primitive is assigned to a distinct, locally homogeneous region. Since a single-peaked Gaussian is inherently suited for homogeneous regions, we guide the placement by evaluating the DC-based cost over candidate split locations, leading to sub-primitives being placed in regions with high DC.

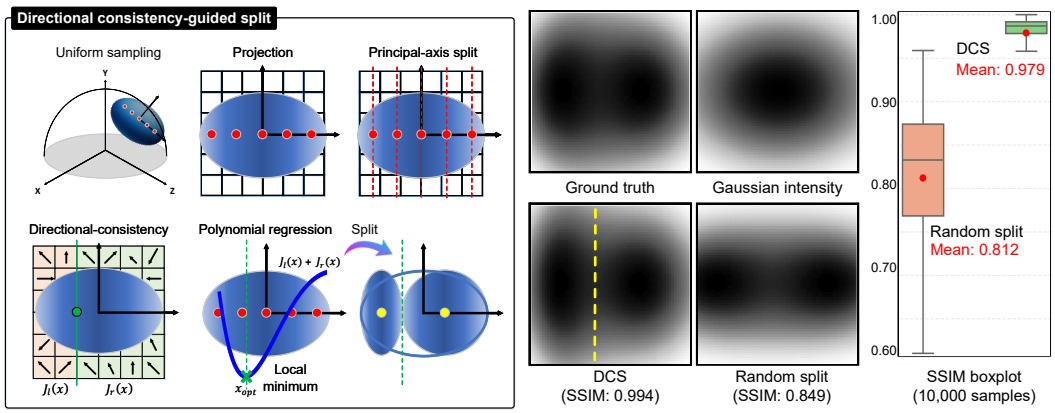

(a) Overview of DCS

(b) Comparison of DCS and random split in 2D

Figure 5: Overview and examples of the DCS. (a) Candidate points are uniformly sampled along the principal axis and projected onto the image plane. The split cost $J(x) = J_l(x) + J_r(x)$ is computed using the directional consistency and gradient magnitudes, and the polynomial regression is used to find the optimal split position x_{opt} from the limited set of discrete samples. (b) In a 2D experimental example, our DCS well aligns the split along the regions structural change occurs, resulting in faithful reconstruction. The plot demonstrates quality statistics in over 10,000 randomized samples.

We constrain candidate split locations to lie along the principal axis of the Gaussian, defined as an axis having the largest scale in the anisotropic matrix S. This axis, p_{local}, is transformed to world coordinates as $p = R \cdot p_{\text{local}}$, using the rotation matrix R of the Gaussian. The split is then performed orthogonally to this axis. Since the principal axis often spans multiple structures, a single elongated primitive exhibits large spatial variance, which increases blur and causes fine details to be smoothed out in structurally distinct regions. This axis-aligned sub-primitive placement mitigates such issues by reducing spatial spread and avoiding the overlaps commonly introduced by random placement, which could otherwise lead to structural discontinuities and incomplete coverage of the pre-split primitives.

To determine the optimal split location, we evaluate the DC-based cost over N candidate locations, placed symmetrically along p relative to the Gaussian center. At each candidate position x, a split line orthogonal to the projected 2D principal axis divides the primitive into left and right sub-regions. For each sub-region, we compute the DC, $\kappa(x)$, and the homodirectional gradient magnitude $\|\hat{g}(x)\|$. The sub-region costs are defined as $J_l(x) = (1 - \kappa_l(x)) \cdot \|\hat{g}_l(x)\|$ and $J_r(x) = (1 - \kappa_r(x)) \cdot \|\hat{g}_r(x)\|$, respectively. The total split cost $J(x)$ is: $J(x) = J_l(x) + J_r(x)$.

Minimizing the DC-based cost facilitates splitting at a point that divides a heterogeneous region into more homogeneous sub-regions, preventing reconstruction sensitivity from being concentrated in a single sub-primitive. Continuously evaluating $J(x)$ is costly in terms of computation and storage, and hence, we employ discrete sampling for efficiency. The overall procedure is illustrated in Fig. 5(a). In our implementation, we empirically set the samples of N=5. Finding the best candidates among the discrete samples can be straightforward, but may require too many samples for a complex junction. To improve this without dense sampling, we polynomially regress the samples [11]. This allows us to efficiently estimate the optimal split location x_{opt} with a minimal number of per-primitive samples; see Appendix A.2 for details.

Notably, the DC-based cost aligns with our DCC in Eq. (3), reinforcing consistent reasoning in the decision to split and the placement of sub-primitives. Although the cost is evaluated before the actual split, minimizing it implicitly guides the sub-primitives toward homogeneous regions, which are less likely to require further splitting.

To validate the effectiveness of DCS, we compare it against random placement using 2D toy examples (see Fig. 5(b)). Here, DCS produces splits that more closely align with the ground truth, and demonstrates more consistent and accurate results over 10,000 randomly generated examples. Its practical effectiveness is demonstrated in Sec. 6.

Algorithm 1 Optimization and Densification
$\|S\|$: maximum Gaussian scale, τ_p, τ_S: thresholds for $\nabla^{DC}_{\mu'} L$ and $\|S\|$, N: number of split candidates

$M, S, R, C, A \leftarrow$ InitAttributes() ▷ Positions, Scales, Rotations, Colors, Opacities
$\nabla^{DC}_{\mu'} L \leftarrow 0$, $k \leftarrow 0$, $\nu \leftarrow 0$ ▷ DC-weighted split criterion, iteration counter, visibility counter
while not converged **do**
  $V, \hat{I} \leftarrow$ SampleTrainingView() ▷ view-projection camera matrix, ground truth
  $I \leftarrow$ Rasterize(M, S, R, C, A, V)
  $L \leftarrow$ Loss$(I, \hat{I})$, $\frac{\partial L}{\partial \mu'} \leftarrow \nabla L$ ▷ backpropagation
  for all Gaussians G_i visible in V **do** ▷ i: index of a Gaussian
    $\nu_i \leftarrow \nu_i + 1$, $\mu_i \leftarrow M_i$
    $\kappa_i \leftarrow$ EvalDirectionalConsistency$(\frac{\partial L}{\partial \mu'_i})$ ▷ Algo. 2
    $\hat{g}_i \leftarrow \sum_j |\frac{\partial L_j}{\partial \mu'_i}|$, $\nabla^{DC}_{\mu'_i} L \leftarrow \nabla^{DC}_{\mu'_i} L + (1 - \kappa_i) \cdot \|\hat{g}_i\|$ ▷ j: pixel position influenced by G_i
    $J_i \leftarrow J_i +$EvalSplitCosts$(\mu_i, S_i, R_i, V, N, \frac{\partial L}{\partial \mu'_i})$ ▷ Algo. 3
  if IsRefinementIteration(k) **then**
    for all Gaussians G_i **do**
      $\nabla^{DC}_{\mu'_i} L \leftarrow (\nabla^{DC}_{\mu'_i} L)/\nu_i$
      if $\nabla^{DC}_{\mu'_i} L > \tau_p$ **and** $\|S_i\| > \tau_S$ **then**
        $x_{\text{opt}} \leftarrow$ PolynomialRegression(J_i, N)
        SplitGaussian$(x_{\text{opt}}, \mu_i, S_i, R_i, C_i, A_i)$ ▷ Algo. 5
      $\nabla^{DC}_{\mu'_i} L \leftarrow 0$, $J_i \leftarrow 0$, $\nu_i \leftarrow 0$
  $M, S, R, C, A \leftarrow$ Adam(∇L), $k \leftarrow k + 1$ ▷ update parameters and increment iteration

5 Implementation details

Our DC4GS can be integrated seamlessly into the existing 3DGS pipelines. We implemented ours on top of the 3DGS [14], as well as its recent extensions: Pixel-GS [44] and AbsGS [38]. Algorithm 1 summarizes the procedure, where yellow-highlighted lines indicate the modifications to the previous ADC schemes. Clone and prune operations are identical to the baselines and thus omitted here.

For each visible Gaussian i, we evaluate its DC κ_i, accumulate its DCC $\nabla^{DC}_{\mu'_i} L$, and estimate its DC-based split cost J_i over N candidate split location samples along the principal axis. The primitive is selected for splitting if its DCC exceeds the gradient threshold τ_p and its maximum scale $\|S_i\|$ is smaller than the scale threshold τ_S. Once selected for splitting, the optimal split location x_{opt} is determined via the polynomial regression over J_i. Additional details are provided in Appendix A.1.

6 Experiments

6.1 Experimental details

Datasets and metrics. We evaluate our DC4GS on the three standard datasets: Mip-NeRF 360 [2] (five outdoor and four indoor scenes), and two scenes each from Tanks and Temples [16] and Deep Blending [12], following the 3DGS [14]. Every 8th frame is used for test. Rendering quality is evaluated by PSNR, SSIM [35], and LPIPS [43]. We also report memory requirements for 3DGS parameters and the number of primitives to assess storage efficiency.

Experimental setup. To ensure a fair comparison with the baselines [14, 38, 44], we adopt their training schedules, loss functions, and all hyperparameters, including the gradient threshold τ_p and the scale threshold τ_S. As with the baselines, we halt the densification after 15K iterations. All the experiments are conducted on a single NVIDIA A6000 GPU with 48GB of memory.

6.2 Comparison with 3DGS-based methods

We compare our DC4GS with the aforementioned baselines by integrating it into their ADCs. Our comparisons with the baselines also include non-3DGS novel-view synthesis methods, including

Table 1: Quantitative comparison of the 3DGS, Pixel-GS, and AbsGS on real-world datasets without and with integrating DC4GS. The results denoted by '*' were excerpted from the 3DGS paper. The rest were obtained through our in-house experiments. The top score, second-highest score, and third-highest score are color-coded in red, orange, and yellow, respectively.

Method	Mip-NeRF360					Tanks&Temples					Deep Blending				
	PSNR ↑	SSIM ↑	LPIPS ↓	Prim.	Mem.	PSNR ↑	SSIM ↑	LPIPS ↓	Prim.	Mem.	PSNR ↑	SSIM ↑	LPIPS ↓	Prim.	Mem.
Plenoxels * [8]	23.080	0.626	0.463	-	2.1GB	21.080	0.719	0.379	-	2.3GB	23.060	0.795	0.510	-	2.7GB
iNGP-big * [25]	25.590	0.699	0.331	-	48MB	21.920	0.745	0.305	-	48MB	24.960	0.817	0.390	-	48MB
Mip-NeRF360 * [2]	27.690	0.792	0.237	-	8.6MB	22.220	0.759	0.257	-	8.6MB	29.400	0.901	0.245	-	8.6MB
3DGS [14]	27.414	0.812	0.218	3350K	792MB	23.655	0.844	0.179	1893K	447MB	29.394	0.898	0.248	2833K	670MB
Scaffold-GS [22]	27.651	0.810	0.226	5460K	164MB	24.018	0.851	0.174	2470K	74MB	30.252	0.904	0.255	1710K	51MB
GES [10]	27.040	0.796	0.248	1543K	365MB	23.640	0.842	0.191	930K	220MB	29.562	0.903	0.249	1606K	380MB
LPM [37]	27.589	0.820	0.212	3426K	810MB	23.878	0.847	0.183	1824K	431MB	29.483	0.901	0.245	2525K	597MB
Pixel-GS [44]	27.537	0.822	0.190	5622K	1329MB	23.759	0.853	0.151	4598K	1087MB	28.812	0.891	0.252	4623K	1093MB
AbsGS [38]	27.504	0.818	0.191	3149K	744MB	23.636	0.852	0.162	1332K	315MB	29.500	0.900	0.237	1961K	463MB
AbsGS (60K iter.)	27.539	0.817	0.189	3162K	748MB	24.039	0.855	0.156	1313K	311MB	29.275	0.895	0.240	1962K	464MB
3DGS+DC4GS	27.486	0.814	0.217	2968K	701MB	23.786	0.845	0.179	1703K	402MB	29.565	0.901	0.245	2644K	625MB
Scaffold-GS+DC4GS	27.653	0.810	0.225	4790K	144MB	24.016	0.849	0.177	2080K	62MB	30.063	0.903	0.257	1350K	40MB
GES+DC4GS	27.090	0.797	0.248	1323K	313MB	23.515	0.841	0.194	816K	193MB	29.632	0.904	0.248	1487K	352MB
LPM+DC4GS	27.556	0.819	0.218	2712K	641MB	23.892	0.846	0.186	1502K	355MB	29.584	0.903	0.244	2350K	555MB
Pixel-GS+DC4GS	27.620	0.824	0.191	5009K	1184MB	23.930	0.855	0.150	4106K	971MB	29.181	0.896	0.246	4284K	1013MB
AbsGS+DC4GS	27.625	0.826	0.188	2615K	618MB	24.121	0.859	0.159	1093K	258MB	29.654	0.905	0.235	1499K	354MB

Mip-NeRF360 [2], iNGP-big [25], and Plenoxels [8]. All the baselines are either re-run using their official implementations with default settings, or taken directly from published results for fairness.

6.2.1 Quantitative comparison

Table 1 shows a quantitative analysis for the three datasets. Overall, when DC4GS is integrated into the baselines [14, 38, 44, 22, 10, 37], it consistently improves them to competitive or superior quality. For Scaffold-GS [22], which does not involve any explicit primitive splitting logic, we only apply our DC-weighted Split Criterion (DCC) and omit the DC-guided Split (DCS). In addition to the quality improvement, DC4GS significantly reduces the number of primitives and memory usage for 3DGS parameters; the largest reduction (on average 20%) is observed in combining our density control with AbsGS, and consistent savings for the other baselines are observed as well. Notably, the combination of DC4GS with AbsGS also yields the greatest improvement in reconstruction quality. DC4GS also achieves up to 11.5% fewer primitives with 3DGS, 11% with Pixel-GS, and 12–18% with Scaffold-GS, GES, and LPM, improving quality metrics. In contrast, simply extending AbsGS training to 60K iterations yields only marginal or even negative gains, indicating that the improvements of DC4GS stem from structural complexity-aware splitting rather than brute-force optimization or longer training (see Table 1).

6.2.2 Training and rendering efficiency comparison

Table 2 compares the training and per-frame rendering times between the baselines and their DC4GS-integrated models. Here, the rendering time is measured by averaging the time taken to render all test-set images for each dataset. The integration of the DC4GS introduces moderate training overhead due to the additional computation of the DC and DC-based cost evaluation. However, this additional cost is confined to training only. At inference time, DC4GS improves rendering efficiency by reducing the number of Gaussian primitives. The consistent speedups in rendering align with the reduced primitive counts, demonstrating the practical scalability of our DC4GS.

6.2.3 Qualitative comparison

Fig. 6 visually compares the improvements achieved by DC4GS. Compared to 3DGS and AbsGS, our DC4GS more faithfully preserves fine structures, such as the window frames, railings, and rods in the figure, where both the baselines often exhibit objectionable discontinuities. It also better maintains object boundaries (the third and last rows), which tend to be oversmoothed in the baselines. While AbsGS generally achieves high visual quality, it is likely to over-split already fine textures, such as the leaves in front of the windows or the grass near rocks (the fourth row), which can result in visual occlusions and structural artifacts. These observations indicate that DC4GS better preserves connected structures such as window frames and railings, which often appear fragmented or discontinuous in the baseline results. It also retains fine details in high-frequency textures, like the leaves or grass, without being occluded by background objects, which is frequently observed in the baselines.

Table 2: Comparison of training time and per-frame rendering time (ms) for the baselines and DC4GS-integrated models on the Mip-NeRF360, Tanks&Temples, and Deep Blending datasets.

Method	Mip-NeRF360		Tanks&Temples		Deep Blending	
	Training	Rendering (ms)	Training	Rendering (ms)	Training	Rendering (ms)
3DGS	**34m**	10.472	**19m**	7.87	**30m**	9.646
3DGS+DC4GS	49m	**9.836**	27m	**7.518**	47m	**9.023**
Scaffold-GS	**1h 1m**	9.705	**29m**	7.015	**42m**	6.298
Scaffold-GS+DC4GS	**1h 1m**	**9.563**	31m	**6.933**	44m	**5.748**
GES	**32m**	6.981	**18m**	5.593	**40m**	6.835
GES+DC4GS	42m	**6.698**	22m	**5.441**	45m	**6.571**
LPM	**38m**	10.702	**18m**	7.143	**30m**	9.090
LPM+DC4GS	54m	**9.462**	27m	**6.370**	49m	**8.512**
Pixel-GS	**49m**	17.163	**35m**	15.212	**41m**	14.271
Pixel-GS+DC4GS	1h 6m	**16.211**	45m	**14.450**	1h 1m	**13.469**
AbsGS	**37m**	9.975	**17m**	6.175	**27m**	7.353
AbsGS (60K iter.)	1h 19m	10.247	38m	6.690	57m	7.549
AbsGS+DC4GS	51m	**9.191**	23m	**5.778**	40m	**6.378**

Figure 6: Qualitative comparison of the baseline methods (3DGS and AbsGS) without and with the integration of our DC4GS. The scenes, from top to bottom, are: Garden, Treehill, Room, Stump, and Bonsai from the Mip-NeRF360 dataset, Truck from the Tanks&Temples, and Playroom from Deep blending dataset.

Table 3: Ablation study evaluating DCC (Sec. 4.2) and DCS (Sec. 4.3) on the Mip-NeRF360, Tanks&Temples, and Deep Blending dataset. The AbsGS [38] is selected as the baseline.

			Mip-NeRF360					Tanks&Temples					Deep Blending				
Baseline	**DCC**	**DCS**	PSNR ↑	SSIM ↑	LPIPS ↓	Prim. ↓	Mem.	PSNR ↑	SSIM ↑	LPIPS ↓	Prim. ↓	Mem.	PSNR ↑	SSIM ↑	LPIPS ↓	Prim. ↓	Mem .
✓			27.504	0.818	0.191	3149K	744MB	23.636	0.852	0.162	1332K	315MB	29.500	0.900	0.237	1961K	463MB
✓	✓		27.507	0.819	0.191	2861K	676MB	23.661	0.852	0.164	1197K	283MB	29.567	0.901	0.237	1799K	425MB
✓		✓	27.587	**0.826**	**0.187**	2877K	680MB	24.018	0.857	**0.158**	1198K	283MB	29.591	**0.905**	**0.235**	1609K	380MB
✓	✓	✓	**27.625**	**0.826**	0.188	**2615K**	618MB	**24.121**	**0.859**	0.159	**1093K**	258MB	**29.654**	**0.905**	**0.235**	**1499K**	354MB

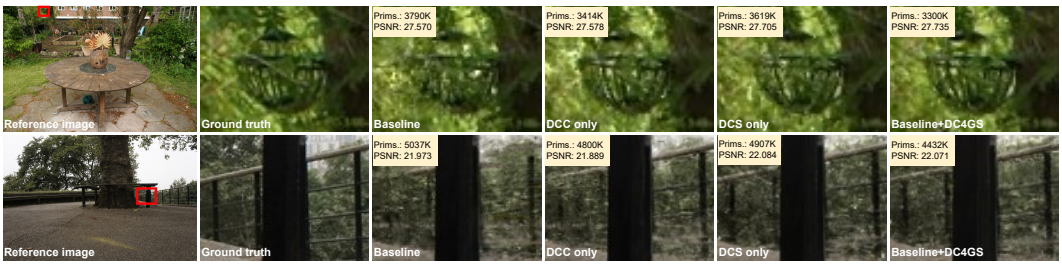

Figure 7: Qualitative visual comparison of our ablation study on the Garden and Treehill scenes from the Mip-NeRF360 dataset.

6.3 Ablation study

To assess the effectiveness of each component, we conduct an ablation study based on the AbsGS baseline [38]. The results are summarized in Table 3.

Directional Consistency-weighted split Criterion (DCC). The effect of applying the DCC (Sec.4.2) is shown in the second row of Table 3. The main effect of DCC is the reduction of the primitive counts. Here, it achieves up to a 24% reduction (Room scene). Notably, it still maintains improved or comparable quality on datasets compared to the baseline.

Directional Consistency-guided Split (DCS). The effect of the DCS (Sec.4.3) appears in the third row of Table 3. Its main effect is the improvement of qualities. Compared to the baseline, the DCS achieves consistently better quality even with fewer primitives.

Combination of DCC and DCS. Combining DCC and DCS is synergistic, which produces the most pronounced improvements. DCC and DCS individually reduce primitives and improve quality, but their integration achieves the fewest primitives and the highest fidelity. In Fig. 7, while each component alleviates artifacts such as occluded or broken cages and railings, their combination better reconstructs fine structures faithfully even with fewer primitives.

7 Conclusion

We introduced DC4GS, a directional consistency-driven density control for 3DGS, which selectively refines primitives by analyzing the angular coherence of positional gradients. Our density control employs directional consistency as a structural cue for both split selection and sub-primitive placement, effectively densifying primitives to align with local structural complexities. We demonstrated that our method can be integrated into the existing 3DGS pipelines and greatly enhances novel-view synthesis quality in diverse scenes with fewer primitives.

Acknowledgement

This work was supported in part by the Mid-career Research Program and CRC Program through the NRF Grants (Nos. RS-2024-00339681 and RS-2023-00221186), and IITP grants (No. RS-2024-00454666), funded by the Korea government (MSIT). Correspondence concerning this article can be addressed to Sungkil Lee.

References

[1] Jonathan T Barron, Ben Mildenhall, Matthew Tancik, Peter Hedman, Ricardo Martin-Brualla, and Pratul P Srinivasan. Mip-nerf: A multiscale representation for anti-aliasing neural radiance fields. In *CVPR*, pages 5855–5864, 2021.

[2] Jonathan T Barron, Ben Mildenhall, Dor Verbin, Pratul P Srinivasan, and Peter Hedman. Mip-nerf 360: Unbounded anti-aliased neural radiance fields. In *CVPR*, pages 5470–5479, 2022.

[3] Jonathan T Barron, Ben Mildenhall, Dor Verbin, Pratul P Srinivasan, and Peter Hedman. Zip-nerf: Anti-aliased grid-based neural radiance fields. In *ICCV*, pages 19697–19705, 2023.

[4] Nicolas Brosse, Alain Durmus, and Eric Moulines. The promises and pitfalls of stochastic gradient langevin dynamics. In *NeurIPS*, volume 31, 2018.

[5] Anpei Chen, Zexiang Xu, Andreas Geiger, Jingyi Yu, and Hao Su. Tensorf: Tensorial radiance fields. In *ECCV*, pages 333–350, 2022.

[6] Zhiqin Chen, Thomas Funkhouser, Peter Hedman, and Andrea Tagliasacchi. Mobilenerf: Exploiting the polygon rasterization pipeline for efficient neural field rendering on mobile architectures. In *CVPR*, 2023.

[7] Ben Fei, Jingyi Xu, Rui Zhang, Qingyuan Zhou, Weidong Yang, and Ying He. 3d gaussian splatting as new era: A survey. *IEEE Transactions on Visualization and Computer Graphics*, 2024.

[8] Sara Fridovich-Keil, Alex Yu, Matthew Tancik, Qinhong Chen, Benjamin Recht, and Angjoo Kanazawa. Plenoxels: Radiance fields without neural networks. In *CVPR*, pages 5501–5510, 2022.

[9] Stephan J Garbin, Marek Kowalski, Matthew Johnson, Jamie Shotton, and Julien Valentin. Fastnerf: High-fidelity neural rendering at 200fps. In *ICCV*, pages 14346–14355, 2021.

[10] Abdullah Hamdi, Luke Melas-Kyriazi, Jinjie Mai, Guocheng Qian, Ruoshi Liu, Carl Vondrick, Bernard Ghanem, and Andrea Vedaldi. Ges: Generalized exponential splatting for efficient radiance field rendering. In *CVPR*, pages 19812–19822, 2024.

[11] Trevor Hastie. *The elements of statistical learning: data mining, inference, and prediction*. Springer, 2009.

[12] Peter Hedman, Julien Philip, True Price, Jan-Michael Frahm, George Drettakis, and Gabriel Brostow. Deep blending for free-viewpoint image-based rendering. *ACM TOG*, 37(6):1–15, 2018.

[13] Letian Huang, Jiayang Bai, Jie Guo, Yuanqi Li, and Yanwen Guo. On the error analysis of 3d gaussian splatting and an optimal projection strategy. In *ECCV*, pages 247–263. Springer, 2024.

[14] Bernhard Kerbl, Georgios Kopanas, Thomas Leimkühler, and George Drettakis. 3d gaussian splatting for real-time radiance field rendering. *ACM TOG*, 42(4):1–14, 2023.

[15] Shakiba Kheradmand, Daniel Rebain, Gopal Sharma, Weiwei Sun, Yang-Che Tseng, Hossam Isack, Abhishek Kar, Andrea Tagliasacchi, and Kwang Moo Yi. 3d gaussian splatting as markov chain monte carlo. In *NeurIPS*, 2024. Spotlight Presentation.

[16] Arno Knapitsch, Jaesik Park, Qian-Yi Zhou, and Vladlen Koltun. Tanks and temples: Benchmarking large-scale scene reconstruction. *ACM TOG*, 36(4):1–13, 2017.

[17] Byeonghyeon Lee, Howoong Lee, Usman Ali, and Eunbyung Park. Sharp-nerf: Grid-based fast deblurring neural radiance fields using sharpness prior. In *IEEE/CVF WACV*, pages 3709–3718, 2024.

[18] Joo Chan Lee, Daniel Rho, Xiangyu Sun, Jong Hwan Ko, and Eunbyung Park. Compact 3d gaussian representation for radiance field. In *CVPR*, pages 21719–21728, 2024.

[19] Jiameng Li, Yue Shi, Jiezhang Cao, Bingbing Ni, Wenjun Zhang, Kai Zhang, and Luc Van Gool. Mipmap-gs: Let gaussians deform with scale-specific mipmap for anti-aliasing rendering. *arXiv preprint arXiv:2408.06286*, 2024.

[20] Tianye Li, Mira Slavcheva, Michael Zollhoefer, Simon Green, Christoph Lassner, Changil Kim, Tanner Schmidt, Steven Lovegrove, Michael Goesele, Richard Newcombe, et al. Neural 3d video synthesis from multi-view video. In *CVPR*, pages 5521–5531, 2022.

[21] Zhihao Liang, Qi Zhang, Wenbo Hu, Lei Zhu, Ying Feng, and Kui Jia. Analytic-splatting: Anti-aliased 3d gaussian splatting via analytic integration. In *ECCV*, pages 281–297. Springer, 2024.

[22] Tao Lu, Mulin Yu, Linning Xu, Yuanbo Xiangli, Limin Wang, Dahua Lin, and Bo Dai. Scaffold-gs: Structured 3d gaussians for view-adaptive rendering. In *CVPR*, pages 20654–20664, 2024.

[23] Kanti V Mardia and Peter E Jupp. *Directional statistics*. John Wiley & Sons, 2009.

[24] Ben Mildenhall, Pratul P. Srinivasan, Matthew Tancik, Jonathan T. Barron, Ravi Ramamoorthi, and Ren Ng. Nerf: Representing scenes as neural radiance fields for view synthesis. In *ECCV*, pages 405–421, 2020.

[25] Thomas Müller, Alex Evans, Christoph Schied, and Alexander Keller. Instant neural graphics primitives with a multiresolution hash encoding. *ACM TOG*, 41(4):1–15, 2022.

[26] Cheng Peng, Yutao Tang, Yifan Zhou, Nengyu Wang, Xijun Liu, Deming Li, and Rama Chellappa. Bags: Blur agnostic gaussian splatting through multi-scale kernel modeling. In *ECCV*, pages 293–310. Springer, 2024.

[27] Albert Pumarola, Enric Corona, Gerard Pons-Moll, and Francesc Moreno-Noguer. D-nerf: Neural radiance fields for dynamic scenes. In *CVPR*, pages 10318–10327, 2021.

[28] Fernando Rivas-Manzaneque, Jorge Sierra-Acosta, Adrian Penate-Sanchez, Francesc Moreno-Noguer, and Angela Ribeiro. Nerflight: Fast and light neural radiance fields using a shared feature grid. In *CVPR*, pages 12417–12427, 2023.

[29] Samuel Rota Bulò, Lorenzo Porzi, and Peter Kontschieder. Revising densification in gaussian splatting. In *ECCV*, pages 347–362. Springer, 2024.

[30] Johannes Lutz Schönberger and Jan-Michael Frahm. Structure-from-motion revisited. In *CVPR*, 2016.

[31] Johannes Lutz Schönberger, Enliang Zheng, Marc Pollefeys, and Jan-Michael Frahm. Pixelwise view selection for unstructured multi-view stereo. In *ECCV*, 2016.

[32] Xiaowei Song, Jv Zheng, Shiran Yuan, Huan-ang Gao, Jingwei Zhao, Xiang He, Weihao Gu, and Hao Zhao. Sa-gs: Scale-adaptive gaussian splatting for training-free anti-aliasing. *arXiv preprint arXiv:2403.19615*, 2024.

[33] Haithem Turki, Vasu Agrawal, Samuel Rota Bulò, Lorenzo Porzi, Peter Kontschieder, Deva Ramanan, Michael Zollhöfer, and Christian Richardt. Hybridnerf: Efficient neural rendering via adaptive volumetric surfaces. In *CVPR*, pages 19647–19656, 2024.

[34] Yuehao Wang, Chaoyi Wang, Bingchen Gong, and Tianfan Xue. Bilateral guided radiance field processing. *ACM TOG*, 43(4):1–13, 2024.

[35] Zhou Wang, Alan C Bovik, Hamid R Sheikh, and Eero P Simoncelli. Image quality assessment: from error visibility to structural similarity. *IEEE TIP*, 13(4):600–612, 2004.

[36] Guanjun Wu, Taoran Yi, Jiemin Fang, Lingxi Xie, Xiaopeng Zhang, Wei Wei, Wenyu Liu, Qi Tian, and Xinggang Wang. 4d gaussian splatting for real-time dynamic scene rendering. In *CVPR*, pages 20310–20320, June 2024.

[37] Haosen Yang, Chenhao Zhang, Wenqing Wang, Marco Volino, Adrian Hilton, Li Zhang, and Xiatian Zhu. Improving gaussian splatting with localized points management. In *CVPR*, pages 21696–21705, 2025.

[38] Zongxin Ye, Wenyu Li, Sidun Liu, Peng Qiao, and Yong Dou. Absgs: Recovering fine details in 3d gaussian splatting. In *ACM MM*, pages 1053–1061, 2024.

[39] Alex Yu, Ruilong Li, Matthew Tancik, Hao Li, Ren Ng, and Angjoo Kanazawa. Plenoctrees for real-time rendering of neural radiance fields. In *ICCV*, pages 5752–5761, 2021.

[40] Zehao Yu, Anpei Chen, Binbin Huang, Torsten Sattler, and Andreas Geiger. Mip-splatting: Alias-free 3d gaussian splatting. In *CVPR*, pages 19447–19456, 2024.

[41] Zehao Yu, Torsten Sattler, and Andreas Geiger. Gaussian opacity fields: Efficient adaptive surface reconstruction in unbounded scenes. *ACM TOG*, 43(6):1–13, 2024.

[42] Jiahui Zhang, Fangneng Zhan, Muyu Xu, Shijian Lu, and Eric Xing. Fregs: 3d gaussian splatting with progressive frequency regularization. In *CVPR*, pages 21424–21433, 2024.

[43] Richard Zhang, Phillip Isola, Alexei A Efros, Eli Shechtman, and Oliver Wang. The unreasonable effectiveness of deep features as a perceptual metric. In *CVPR*, pages 586–595, 2018.

[44] Zheng Zhang, Wenbo Hu, Yixing Lao, Tong He, and Hengshuang Zhao. Pixel-gs: Density control with pixel-aware gradient for 3d gaussian splatting. In *ECCV*, pages 326–342. Springer, 2024.

NeurIPS Paper Checklist

1. **Claims**

   Question: Do the main claims made in the abstract and introduction accurately reflect the paper's contributions and scope?

   Answer: [Yes]

   Justification: The abstract and introduction both provide a thorough explanation of our claims.

   Guidelines:

   - The answer NA means that the abstract and introduction do not include the claims made in the paper.
   - The abstract and/or introduction should clearly state the claims made, including the contributions made in the paper and important assumptions and limitations. A No or NA answer to this question will not be perceived well by the reviewers.
   - The claims made should match theoretical and experimental results, and reflect how much the results can be expected to generalize to other settings.
   - It is fine to include aspirational goals as motivation as long as it is clear that these goals are not attained by the paper.

2. **Limitations**

   Question: Does the paper discuss the limitations of the work performed by the authors?

   Answer: [Yes]

   Justification: We discuss the limitation of our work in Appendix A.4.

   Guidelines:

   - The answer NA means that the paper has no limitation while the answer No means that the paper has limitations, but those are not discussed in the paper.
   - The authors are encouraged to create a separate "Limitations" section in their paper.
   - The paper should point out any strong assumptions and how robust the results are to violations of these assumptions (e.g., independence assumptions, noiseless settings, model well-specification, asymptotic approximations only holding locally). The authors should reflect on how these assumptions might be violated in practice and what the implications would be.
   - The authors should reflect on the scope of the claims made, e.g., if the approach was only tested on a few datasets or with a few runs. In general, empirical results often depend on implicit assumptions, which should be articulated.
   - The authors should reflect on the factors that influence the performance of the approach. For example, a facial recognition algorithm may perform poorly when image resolution is low or images are taken in low lighting. Or a speech-to-text system might not be used reliably to provide closed captions for online lectures because it fails to handle technical jargon.
   - The authors should discuss the computational efficiency of the proposed algorithms and how they scale with dataset size.
   - If applicable, the authors should discuss possible limitations of their approach to address problems of privacy and fairness.
   - While the authors might fear that complete honesty about limitations might be used by reviewers as grounds for rejection, a worse outcome might be that reviewers discover limitations that aren't acknowledged in the paper. The authors should use their best judgment and recognize that individual actions in favor of transparency play an important role in developing norms that preserve the integrity of the community. Reviewers will be specifically instructed to not penalize honesty concerning limitations.

3. **Theory assumptions and proofs**

   Question: For each theoretical result, does the paper provide the full set of assumptions and a complete (and correct) proof?

   Answer: [NA]

Justification: This paper focuses on empirical findings rather than theoretical analysis; hence, no formal theorems or proofs are included.

Guidelines:

- The answer NA means that the paper does not include theoretical results.
- All the theorems, formulas, and proofs in the paper should be numbered and cross-referenced.
- All assumptions should be clearly stated or referenced in the statement of any theorems.
- The proofs can either appear in the main paper or the supplemental material, but if they appear in the supplemental material, the authors are encouraged to provide a short proof sketch to provide intuition.
- Inversely, any informal proof provided in the core of the paper should be complemented by formal proofs provided in appendix or supplemental material.
- Theorems and Lemmas that the proof relies upon should be properly referenced.

4. **Experimental result reproducibility**

   Question: Does the paper fully disclose all the information needed to reproduce the main experimental results of the paper to the extent that it affects the main claims and/or conclusions of the paper (regardless of whether the code and data are provided or not)?

   Answer: [Yes]

   Justification: We provide implementation details in Sec. 5 and Appendix A.1, and include the implementation code in the supplementary material.

   Guidelines:

   - The answer NA means that the paper does not include experiments.
   - If the paper includes experiments, a No answer to this question will not be perceived well by the reviewers: Making the paper reproducible is important, regardless of whether the code and data are provided or not.
   - If the contribution is a dataset and/or model, the authors should describe the steps taken to make their results reproducible or verifiable.
   - Depending on the contribution, reproducibility can be accomplished in various ways. For example, if the contribution is a novel architecture, describing the architecture fully might suffice, or if the contribution is a specific model and empirical evaluation, it may be necessary to either make it possible for others to replicate the model with the same dataset, or provide access to the model. In general. releasing code and data is often one good way to accomplish this, but reproducibility can also be provided via detailed instructions for how to replicate the results, access to a hosted model (e.g., in the case of a large language model), releasing of a model checkpoint, or other means that are appropriate to the research performed.
   - While NeurIPS does not require releasing code, the conference does require all submissions to provide some reasonable avenue for reproducibility, which may depend on the nature of the contribution. For example
     (a) If the contribution is primarily a new algorithm, the paper should make it clear how to reproduce that algorithm.
     (b) If the contribution is primarily a new model architecture, the paper should describe the architecture clearly and fully.
     (c) If the contribution is a new model (e.g., a large language model), then there should either be a way to access this model for reproducing the results or a way to reproduce the model (e.g., with an open-source dataset or instructions for how to construct the dataset).
     (d) We recognize that reproducibility may be tricky in some cases, in which case authors are welcome to describe the particular way they provide for reproducibility. In the case of closed-source models, it may be that access to the model is limited in some way (e.g., to registered users), but it should be possible for other researchers to have some path to reproducing or verifying the results.

5. **Open access to data and code**

Question: Does the paper provide open access to the data and code, with sufficient instructions to faithfully reproduce the main experimental results, as described in supplemental material?

Answer: [No]

Justification: The datasets we use are publicly available, and we plan to release our code as well.

Guidelines:

- The answer NA means that paper does not include experiments requiring code.
- Please see the NeurIPS code and data submission guidelines (`https://nips.cc/public/guides/CodeSubmissionPolicy`) for more details.
- While we encourage the release of code and data, we understand that this might not be possible, so "No" is an acceptable answer. Papers cannot be rejected simply for not including code, unless this is central to the contribution (e.g., for a new open-source benchmark).
- The instructions should contain the exact command and environment needed to run to reproduce the results. See the NeurIPS code and data submission guidelines (`https://nips.cc/public/guides/CodeSubmissionPolicy`) for more details.
- The authors should provide instructions on data access and preparation, including how to access the raw data, preprocessed data, intermediate data, and generated data, etc.
- The authors should provide scripts to reproduce all experimental results for the new proposed method and baselines. If only a subset of experiments are reproducible, they should state which ones are omitted from the script and why.
- At submission time, to preserve anonymity, the authors should release anonymized versions (if applicable).
- Providing as much information as possible in supplemental material (appended to the paper) is recommended, but including URLs to data and code is permitted.

6. **Experimental setting/details**

   Question: Does the paper specify all the training and test details (e.g., data splits, hyperparameters, how they were chosen, type of optimizer, etc.) necessary to understand the results?

   Answer: [Yes]

   Justification: We report the detailed training and test details in Sec. 6.1

   Guidelines:

   - The answer NA means that the paper does not include experiments.
   - The experimental setting should be presented in the core of the paper to a level of detail that is necessary to appreciate the results and make sense of them.
   - The full details can be provided either with the code, in appendix, or as supplemental material.

7. **Experiment statistical significance**

   Question: Does the paper report error bars suitably and correctly defined or other appropriate information about the statistical significance of the experiments?

   Answer: [Yes]

   Justification: We provide boxplots in Fig. 5(b) and Fig. 8, summarizing the distribution of performance over 10,000 samples. However, we do not perform multiple training runs of 3DGS-based methods due to limited computational resources.

   Guidelines:

   - The answer NA means that the paper does not include experiments.
   - The authors should answer "Yes" if the results are accompanied by error bars, confidence intervals, or statistical significance tests, at least for the experiments that support the main claims of the paper.

- The factors of variability that the error bars are capturing should be clearly stated (for example, train/test split, initialization, random drawing of some parameter, or overall run with given experimental conditions).
- The method for calculating the error bars should be explained (closed form formula, call to a library function, bootstrap, etc.)
- The assumptions made should be given (e.g., Normally distributed errors).
- It should be clear whether the error bar is the standard deviation or the standard error of the mean.
- It is OK to report 1-sigma error bars, but one should state it. The authors should preferably report a 2-sigma error bar than state that they have a 96% CI, if the hypothesis of Normality of errors is not verified.
- For asymmetric distributions, the authors should be careful not to show in tables or figures symmetric error bars that would yield results that are out of range (e.g. negative error rates).
- If error bars are reported in tables or plots, The authors should explain in the text how they were calculated and reference the corresponding figures or tables in the text.

8. **Experiments compute resources**

   Question: For each experiment, does the paper provide sufficient information on the computer resources (type of compute workers, memory, time of execution) needed to reproduce the experiments?

   Answer: [Yes]

   Justification: Please refer to Sec. 6.1, Table 1, and Appendix 6.2.2.

   Guidelines:

   - The answer NA means that the paper does not include experiments.
   - The paper should indicate the type of compute workers CPU or GPU, internal cluster, or cloud provider, including relevant memory and storage.
   - The paper should provide the amount of compute required for each of the individual experimental runs as well as estimate the total compute.
   - The paper should disclose whether the full research project required more compute than the experiments reported in the paper (e.g., preliminary or failed experiments that didn't make it into the paper).

9. **Code of ethics**

   Question: Does the research conducted in the paper conform, in every respect, with the NeurIPS Code of Ethics `https://neurips.cc/public/EthicsGuidelines`?

   Answer: [Yes]

   Justification: Our research in this paper conforms to the NeurIPS Code of Ethics.

   Guidelines:

   - The answer NA means that the authors have not reviewed the NeurIPS Code of Ethics.
   - If the authors answer No, they should explain the special circumstances that require a deviation from the Code of Ethics.
   - The authors should make sure to preserve anonymity (e.g., if there is a special consideration due to laws or regulations in their jurisdiction).

10. **Broader impacts**

    Question: Does the paper discuss both potential positive societal impacts and negative societal impacts of the work performed?

    Answer: [Yes]

    Justification: Although our work primarily addresses foundational methods for 3D reconstruction, we briefly discuss potential societal impacts in Appendix A.5

    Guidelines:

    - The answer NA means that there is no societal impact of the work performed.

- If the authors answer NA or No, they should explain why their work has no societal impact or why the paper does not address societal impact.
- Examples of negative societal impacts include potential malicious or unintended uses (e.g., disinformation, generating fake profiles, surveillance), fairness considerations (e.g., deployment of technologies that could make decisions that unfairly impact specific groups), privacy considerations, and security considerations.
- The conference expects that many papers will be foundational research and not tied to particular applications, let alone deployments. However, if there is a direct path to any negative applications, the authors should point it out. For example, it is legitimate to point out that an improvement in the quality of generative models could be used to generate deepfakes for disinformation. On the other hand, it is not needed to point out that a generic algorithm for optimizing neural networks could enable people to train models that generate Deepfakes faster.
- The authors should consider possible harms that could arise when the technology is being used as intended and functioning correctly, harms that could arise when the technology is being used as intended but gives incorrect results, and harms following from (intentional or unintentional) misuse of the technology.
- If there are negative societal impacts, the authors could also discuss possible mitigation strategies (e.g., gated release of models, providing defenses in addition to attacks, mechanisms for monitoring misuse, mechanisms to monitor how a system learns from feedback over time, improving the efficiency and accessibility of ML).

11. **Safeguards**

    Question: Does the paper describe safeguards that have been put in place for responsible release of data or models that have a high risk for misuse (e.g., pretrained language models, image generators, or scraped datasets)?

    Answer: [NA]

    Justification: The paper does not pose such risks, as it does not involve any models or data associated with privacy concerns.

    Guidelines:

    - The answer NA means that the paper poses no such risks.
    - Released models that have a high risk for misuse or dual-use should be released with necessary safeguards to allow for controlled use of the model, for example by requiring that users adhere to usage guidelines or restrictions to access the model or implementing safety filters.
    - Datasets that have been scraped from the Internet could pose safety risks. The authors should describe how they avoided releasing unsafe images.
    - We recognize that providing effective safeguards is challenging, and many papers do not require this, but we encourage authors to take this into account and make a best faith effort.

12. **Licenses for existing assets**

    Question: Are the creators or original owners of assets (e.g., code, data, models), used in the paper, properly credited and are the license and terms of use explicitly mentioned and properly respected?

    Answer: [Yes]

    Justification: Please refer to Appendix A.6.

    Guidelines:

    - The answer NA means that the paper does not use existing assets.
    - The authors should cite the original paper that produced the code package or dataset.
    - The authors should state which version of the asset is used and, if possible, include a URL.
    - The name of the license (e.g., CC-BY 4.0) should be included for each asset.
    - For scraped data from a particular source (e.g., website), the copyright and terms of service of that source should be provided.

- If assets are released, the license, copyright information, and terms of use in the package should be provided. For popular datasets, `paperswithcode.com/datasets` has curated licenses for some datasets. Their licensing guide can help determine the license of a dataset.
- For existing datasets that are re-packaged, both the original license and the license of the derived asset (if it has changed) should be provided.
- If this information is not available online, the authors are encouraged to reach out to the asset's creators.

13. **New assets**

    Question: Are new assets introduced in the paper well documented and is the documentation provided alongside the assets?

    Answer: [NA]

    Justification: We do not provide new assets.

    Guidelines:

    - The answer NA means that the paper does not release new assets.
    - Researchers should communicate the details of the dataset/code/model as part of their submissions via structured templates. This includes details about training, license, limitations, etc.
    - The paper should discuss whether and how consent was obtained from people whose asset is used.
    - At submission time, remember to anonymize your assets (if applicable). You can either create an anonymized URL or include an anonymized zip file.

14. **Crowdsourcing and research with human subjects**

    Question: For crowdsourcing experiments and research with human subjects, does the paper include the full text of instructions given to participants and screenshots, if applicable, as well as details about compensation (if any)?

    Answer: [NA]

    Justification: This work does not involve any crowdsourcing or studies involving human subjects.

    Guidelines:

    - The answer NA means that the paper does not involve crowdsourcing nor research with human subjects.
    - Including this information in the supplemental material is fine, but if the main contribution of the paper involves human subjects, then as much detail as possible should be included in the main paper.
    - According to the NeurIPS Code of Ethics, workers involved in data collection, curation, or other labor should be paid at least the minimum wage in the country of the data collector.

15. **Institutional review board (IRB) approvals or equivalent for research with human subjects**

    Question: Does the paper describe potential risks incurred by study participants, whether such risks were disclosed to the subjects, and whether Institutional Review Board (IRB) approvals (or an equivalent approval/review based on the requirements of your country or institution) were obtained?

    Answer: [NA]

    Justification: We do not conduct any user studies or involve human subjects.

    Guidelines:

    - The answer NA means that the paper does not involve crowdsourcing nor research with human subjects.
    - Depending on the country in which research is conducted, IRB approval (or equivalent) may be required for any human subjects research. If you obtained IRB approval, you should clearly state this in the paper.

- We recognize that the procedures for this may vary significantly between institutions and locations, and we expect authors to adhere to the NeurIPS Code of Ethics and the guidelines for their institution.
- For initial submissions, do not include any information that would break anonymity (if applicable), such as the institution conducting the review.

16. **Declaration of LLM usage**

    Question: Does the paper describe the usage of LLMs if it is an important, original, or non-standard component of the core methods in this research? Note that if the LLM is used only for writing, editing, or formatting purposes and does not impact the core methodology, scientific rigorousness, or originality of the research, declaration is not required.

    Answer: [NA]

    Justification: LLMs were not used in the core methodology; any usage was limited to minor writing assistance without affecting the technical content.

    Guidelines:

    - The answer NA means that the core method development in this research does not involve LLMs as any important, original, or non-standard components.
    - Please refer to our LLM policy (`https://neurips.cc/Conferences/2025/LLM`) for what should or should not be described.

A Appendix

A.1 Additional implementation details

This section provides detailed implementation components that support the overall optimization and densification process summarized in Algo. 1 of Sec. 5. Specifically, we describe the key modules in DC4GS: the evaluation of the directional consistency (DC), DC-based split costs, and the generation of sub-primitives. Each corresponds to a modified line in Algo. 1, and is detailed in the following subsections with standalone pseudocode for clarity and reproducibility.

A.1.1 Directional consistency

Algorithm 2 Directional consistency (DC) from positional gradients
$\frac{\partial L}{\partial \mu'}$: positional gradients w.r.t. projected Gaussian center μ'

function EvalDirectionalConsistency($\frac{\partial L}{\partial \mu'}$)
  $N \leftarrow 0$
  for all $g \in \frac{\partial L}{\partial \mu'}$ **do**
    $N \leftarrow N + 1$
    $u \leftarrow u + \frac{g}{\|g\|}$ ▷ accumulate unit vector of positional gradient
  $C \leftarrow \frac{1}{N} u$ ▷ circular mean
  return $\|C\|$ ▷ DC
end function

Algo. 2 presents the implementation of the DC defined in Section 4.1. Given a set of 2D positional gradients $\frac{\partial L}{\partial \mu'}$, where each gradient corresponds to a pixel affected by the Gaussian, we first normalize each gradient to obtain a unit vector indicating its direction. These unit vectors are accumulated and averaged to form the circular mean C. The directional consistency κ is then computed as the L2 norm $\|C\|$ of this mean vector.

A.1.2 DC-based split cost

Algorithm 3 DC-based split costs for N (odd) candidates along the principal axis.
μ, S, R: Gaussian center, scale, rotation; V: view-projection matrix

function EvalSplitCosts(μ, S, R, V, N, $\frac{\partial L}{\partial \mu'}$)
  $a \leftarrow \arg\max_{i \in \{x,y,z\}} S(i)$ ▷ select principal axis
  $p_{\text{local}} \leftarrow \mathbf{e}(a)$ ▷ basis vector along axis a
  $p \leftarrow R \cdot p_{\text{local}}$ ▷ axis in world space
  $d \leftarrow 6 \cdot S(a)$ ▷ diameter of a gaussian
  $x^{3D}_{\text{end}} \leftarrow \mu + 0.5d \cdot p$ ▷ end point of the principal axis
  $x^{2D}_{\text{end}} \leftarrow$ Project2D(x^{3D}_{end}, V)
  $\delta \leftarrow d/(N+1)$ ▷ sampling interval
  $J \leftarrow \emptyset$, $K \leftarrow \lfloor N/2 \rfloor$
  for $i = -K$ to $+K$ **do**
    $x^{3D}_i \leftarrow \mu + i \cdot \delta \cdot p$, $x^{2D}_i \leftarrow$ Project2D(x^{3D}_i, V)
    $J \leftarrow J \cup$CostAt(x^{2D}_i,x^{2D}_{end},$\frac{\partial L}{\partial \mu'}$) ▷ Alg. 4
  return J
end function

Algo. 3 and 4 implement the DC-based cost evaluation process for the directional consistency-guided split (DCS), as described in Sec. 4.3.

Algo. 3 samples N candidate split points symmetrically along the principal axis of a Gaussian, defined as the direction of maximal scale in the anisotropic matrix S and transformed to world coordinates via the rotation matrix R. Each 3D candidate point x^{3D} is projected into image space using the

Algorithm 4 DC-based cost for a candidate split
x_k: split point, x_{end}: principal axis endpoint, (x, g): pixel position and gradient

function CostAt(x_k, x_{end}, $\frac{\partial L}{\partial \mu'}$)
  $\mathbf{v}_{\text{axis}} \leftarrow x_{\text{end}} - x_k$ ▷ 2D principal axis direction
  $\mathcal{P}_l \leftarrow []$, $\mathcal{P}_r \leftarrow []$, $\hat{g}_l \leftarrow 0$, $\hat{g}_r \leftarrow 0$
  for all $(x, g) \in \frac{\partial L}{\partial \mu'}$ **do**
    $\mathbf{v}_{\text{pix}} \leftarrow x - x_k$, $d \leftarrow \mathbf{v}_{\text{axis}} \cdot \mathbf{v}_{\text{pix}}$ ▷ dot product to determine side of split
    if $d < 0$ **then** ▷ left of split line
      $\mathcal{P}_l \leftarrow \mathcal{P}_l \cup \{g\}$, $\hat{g}_l \leftarrow \hat{g}_l + |g|$
    else ▷ right of split line
      $\mathcal{P}_r \leftarrow \mathcal{P}_r \cup \{g\}$, $\hat{g}_r \leftarrow \hat{g}_r + |g|$
  $\kappa_l \leftarrow$ EvalDirectionalConsistency($\mathcal{P}_l$), $\kappa_r \leftarrow$ EvalDirectionalConsistency($\mathcal{P}_r$) ▷ Alg. 2
  $J_l \leftarrow (1 - \kappa_l) \cdot \|\hat{g}_l\|$, $J_r \leftarrow (1 - \kappa_r) \cdot \|\hat{g}_r\|$
  return $J_l + J_r$
end function

view-projection matrix V, and the corresponding DC-based cost is computed at each x^{2D} using Algo. 4.

Algo. 4 computes the cost for a single split point x_k (i.e., x^{2D} from Algo. 3). A split line orthogonal to the projected principal axis divides the affected pixels into left and right subsets. For each subset, the DC κ is evaluated using Algo. 2, and the gradients $|g|$ are accumulated. The cost for each side is computed as $(1 - \kappa) \cdot \|\hat{g}\|$, and the final cost is the sum of both sides.

A.1.3 Sub-primitive generation in DCS

Algorithm 5 Splits a Gaussian into sub-primitives at x_{opt}
μ, S, R, c, o,: center, scale, rotation, color, and opacity of a Gaussian

function SplitGaussian(x_{opt}, μ, S, R, c, o)
  $a \leftarrow \arg\max_{i \in \{x,y,z\}} S(i)$ ▷ select principal axis
  $p_{\text{local}} \leftarrow \mathbf{e}(a)$, $p \leftarrow R \cdot p_{\text{local}}$ ▷ axis in world space
  $d \leftarrow 6 \cdot s(a)$ ▷ diameter of a gaussian
  $d_l \leftarrow d \cdot (1 - x_{\text{opt}})$, $d_r \leftarrow d \cdot x_{\text{opt}}$
  $\mu_l \leftarrow \mu - (d_l/2) \cdot p$, $\mu_r \leftarrow \mu + (d_r/2) \cdot p$
  $S_l \leftarrow S$, $S_l(a) \leftarrow S_l(a) \cdot x_{\text{opt}}$
  $S_r \leftarrow S$, $S_r(a) \leftarrow S_r(a) \cdot (1 - x_{\text{opt}})$
  $o_l \leftarrow o \cdot x_{\text{opt}}$, $o_r \leftarrow o \cdot (1 - x_{\text{opt}})$
  $G_l \leftarrow Gaussain(\mu_l, S_l, R, c, o_l)$, $G_r \leftarrow Gaussain(\mu_r, S_r, R, c, o_r)$
  $G \leftarrow G \cup (G_l \cup G_r)$ ▷ add sub-primitives to the Gaussian set
end function

Algo. 5 implements the sub-primitive generation step after determining the optimal split position x_{opt}. This operation spawns two new Gaussians by dividing the original one along its principal axis.

To perform this split, the function computes the left and right extents from the center based on the optimal split position x_{opt}, using the principal axis direction defined during cost evaluation (see Algo. 3). The new centers μ_l and μ_r are offset from the original center μ, and the corresponding scales along the principal axis are proportionally adjusted to x_{opt} and $1 - x_{\text{opt}}$. Opacity values are also redistributed in the same ratio to avoid unintentionally increasing or decreasing the overall density of the original Gaussian. Each resulting sub-primitive retains the original rotation and color and is subsequently added to the primitive set.

A.1.4 Training-time overhead analysis

In practice, DC4GS reduces the number of primitives, which accelerates the rendering time. To quantify the computational trade-offs, we provide a breakdown of DC-related overhead in Table 4.

Table 4: Breakdown of per-iteration training-time overhead introduced by DC4GS, measured on the bicycle scene of Mip-NeRF360 dataset.

Module	Time (ms)
Directional Consistency (DC) evaluation	0.010
DC-based split cost computation	31.020
Sub-primitive generation	16.913
Total Additional Overhead	**47.943**

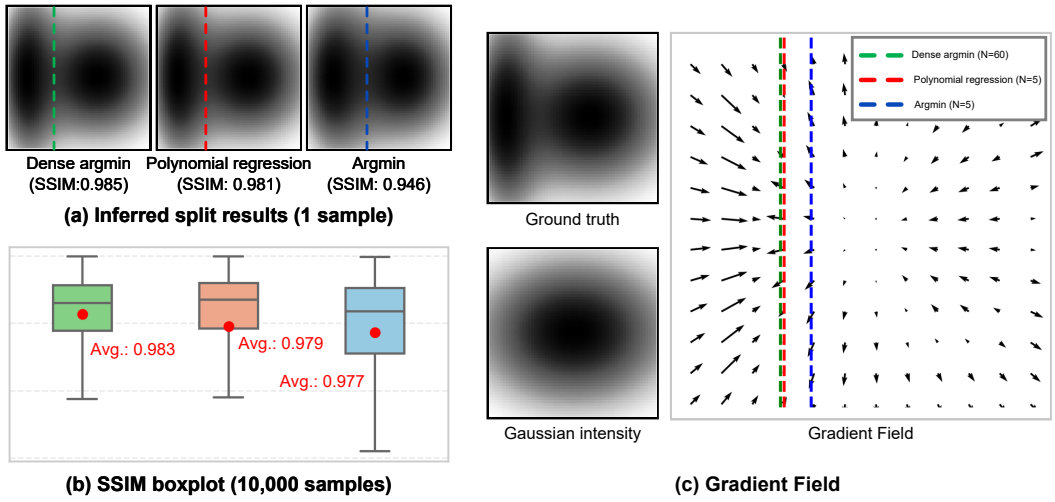

Figure 8: Comparison of split location selection strategies in our consistency-guided split using synthetic toy examples. (a) On a synthetic sample, we compare three strategies: dense argmin (N=60), polynomial regression (N=5), and argmin (N=5). Dense and regression methods yield sub-primitives well-aligned with the ground truth and capture structural boundaries where gradient directions conflict (see gradient field), while argmin slightly overextends the left side. (b) SSIM boxplots over 10,000 samples. Regression achieves near-equal accuracy to dense argmin. It outperforms argmin in accuracy and stability (tighter IQR), demonstrating robust performance under limited sampling.

These results are based on the Mip-NeRF360 bicycle scene with 44,206 primitives. This breakdown clarifies that most of the overhead arises from atomic operations in DC-based splitting.

A.2 Effect of sampling resolution and selection method

We evaluate how the accuracy of split estimation is affected by the sampling resolution N and the choice of selection method in our DCS. We compare three settings: 1) dense argmin (N=60), 2) polynomial regression [11] over N=5 candidates, and 3) sparse argmin (N=5).

Fig. 8(a) shows a synthetic example where both the dense argmin and regression identify the structural boundary well, while the sparse argmin misplaces the split, slightly overextending to the left. As shown in Fig. 8(c), this boundary aligns with a region where gradient directions conflict. The regression successfully detects this transition, preserving the underlying structure.

Fig. 8(b) shows SSIM boxplots over 10,000 samples. Dense argmin achieves the highest average (0.983), followed by the regression (0.979) and sparse argmin (0.977). The regression also exhibits the tightest distribution (median=0.987, IQR (InterQuartile Range)=0.0136), outperforming the sparse argmin (median=0.983, IQR=0.0194). These results confirm that the regression provides accurate and stable split estimation, even under limited sampling.

Table 5: Quantitative comparison for the Mip-NeRF360 scenes. From the top row to the bottom row, the results indicate PSNR, SSIM, LPIPS, and the number of primitives, respectively.

Model	bicycle	bonsai	counter	flowers	garden	kitchen	room	stump	treehill
3DGS [14]	25.1331	**32.1688**	**29.0042**	21.4235	27.2435	31.3263	31.3873	26.5487	**22.4933**
3DGS+DC4GS	**25.1866**	32.1594	28.9499	**21.5535**	**27.3492**	**31.4530**	**31.6532**	**26.6118**	22.4582
Pixel-GS [44]	25.2318	**32.5194**	29.1654	21.5205	27.3366	31.6594	31.4681	26.8150	22.1198
Pixel-GS+DC4GS	**25.3140**	32.4600	**29.1790**	**21.7308**	**27.4599**	**31.6957**	**31.5255**	**26.8978**	**22.3223**
AbsGS [38]	25.2407	**32.3531**	**29.1104**	21.1861	27.5704	**31.8096**	**31.6676**	26.6322	21.9733
AbsGS+DC4GS	**25.5344**	32.2905	29.0290	**21.5621**	**27.7356**	31.7880	31.6649	**26.9562**	**22.0716**

Model	bicycle	bonsai	counter	flowers	garden	kitchen	room	stump	treehill
3DGS	0.7602	**0.9400**	**0.9061**	0.6019	0.8619	0.9259	0.9178	0.7691	0.6307
3DGS+DC4GS	**0.7655**	0.9399	0.9060	**0.6059**	**0.8638**	**0.9261**	**0.9188**	**0.7743**	**0.6331**
Pixel-GS	0.7757	**0.9445**	0.9121	0.6337	0.8661	0.9292	0.9206	0.7836	0.6316
Pixel-GS+DC4GS	**0.7798**	0.9442	**0.9122**	**0.6403**	**0.8680**	**0.9293**	**0.9212**	**0.7876**	**0.6375**
AbsGS	0.7800	0.9453	**0.9120**	0.6174	0.8713	0.9297	**0.9253**	0.7753	0.6133
AbsGS+DC4GS	**0.7925**	**0.9445**	0.9113	**0.6348**	**0.8741**	**0.9300**	0.9252	**0.7924**	**0.6287**

Model	bicycle	bonsai	counter	flowers	garden	kitchen	room	stump	treehill
3DGS	0.2159	**0.2050**	**0.2019**	0.3411	0.1092	**0.1265**	0.2197	0.2186	**0.3292**
3DGS+DC4GS	**0.2104**	0.2058	0.2026	**0.3366**	**0.1083**	0.1267	**0.2189**	**0.2142**	0.3310
Pixel-GS	0.1818	**0.1934**	**0.1844**	**0.2617**	0.1003	**0.1195**	0.2110	0.1868	**0.2787**
Pixel-GS+DC4GS	**0.1793**	0.1938	0.1857	0.2654	**0.0996**	0.1199	**0.2105**	**0.1858**	0.2848
AbsGS	0.1729	**0.1894**	**0.1874**	0.2713	0.0992	**0.1206**	**0.1999**	0.1979	0.2801
AbsGS+DC4GS	**0.1663**	0.1907	0.1892	**0.2684**	**0.0977**	0.1211	0.2018	**0.1884**	**0.2733**

Model	bicycle	bonsai	counter	flowers	garden	kitchen	room	stump	treehill
3DGS	6056K	1285K	1226K	3618K	5694K	1839K	1592K	4895K	3944K
3DGS+DC4GS	**5299K**	**1124K**	**1112K**	**3389K**	**5269K**	**1677K**	**1419K**	**3980K**	**3438K**
Pixel-GS	9028K	2102K	2603K	7517K	8574K	3180K	2588K	6610K	8396K
Pixel-GS+DC4GS	**8047K**	**1860K**	**2378K**	**6966K**	**7914K**	**2945K**	**2332K**	**5730K**	**6906K**
AbsGS	6051K	1045K	970K	3886K	3790K	1243K	1471K	4845K	5037K
AbsGS+DC4GS	**5021K**	**830K**	**754K**	**3330K**	**3300K**	**930K**	**1036K**	**3898K**	**4432K**

Table 6: Quantitative comparison for the Tanks&Temples scenes. From the top row to the bottom row, the results indicate PSNR, SSIM, LPIPS, and the number of primitives (Prim.), respectively.

Method	Train				Truck			
	PSNR ↑	SSIM ↑	LPIPS ↓	Prim.	PSNR ↑	SSIM ↑	LPIPS ↓	Prim.
3DGS	21.8415	0.8103	**0.2103**	1099K	25.4690	0.8777	0.1486	2687K
3DGS+DC4GS	**21.9974**	**0.8116**	0.2112	**1048K**	**25.5747**	**0.8801**	**0.1469**	**2358K**
Pixel-GS	21.9925	0.8236	0.1804	3857K	25.5262	0.8828	0.1216	5338K
Pixel-GS+DC4GS	**22.2010**	**0.8260**	**0.1799**	**3561K**	**25.6590**	**0.8856**	**0.1213**	**4650K**
AbsGS	21.5800	0.8178	0.1927	1008K	25.6926	0.8869	0.1322	1657K
AbsGS+DC4GS	**22.3767**	**0.8291**	**0.1871**	**787K**	**25.8666**	**0.8894**	**0.1317**	**1399K**

Table 7: Quantitative comparison for the Deep Blending scenes. From the top row to the bottom row, the results indicate PSNR, SSIM, LPIPS, and the number of primitives (Prim.), respectively.

Method	Dr Johnson				Playroom			
	PSNR ↑	SSIM ↑	LPIPS ↓	Prim.	PSNR ↑	SSIM ↑	LPIPS ↓	Prim.
3DGS	29.0423	0.8977	0.2471	3321K	29.7464	0.8997	0.2490	2345K
3DGS+DC4GS	**29.1892**	**0.9000**	**0.2455**	**3158K**	**29.9417**	**0.9021**	**0.2459**	**2131K**
Pixel-GS	27.9112	0.8843	0.2602	5491K	29.7131	0.8989	0.2446	3754K
Pixel-GS+DC4GS	**28.5347**	**0.8914**	**0.2500**	**5203K**	**29.8276**	**0.9010**	**0.2429**	**3365K**
AbsGS	29.0475	0.8956	0.2420	2455K	29.9527	0.9049	**0.2330**	1467K
AbsGS+DC4GS	**29.2328**	**0.9027**	**0.2370**	**1905K**	**30.0759**	**0.9087**	0.2331	**1093K**

A.3 Additional experimental results

A.3.1 Per-scene quantitative results

Tables 5–7 report detailed per-scene metrics, including PSNR, SSIM, LPIPS, and the number of primitives, for all datasets. The results show that DC4GS consistently reduces the number of primitives and maintains or improves reconstruction quality compared to each baseline method.

In the stump scene, applying DC4GS to 3DGS results in up to a 19% reduction in primitives. With Pixel-GS [44], DC4GS achieves up to an 18% reduction in the treehill scene. The largest reduction is observed with AbsGS [38], where DC4GS reduces the number of primitives by up to 30% in the room scene. In all cases, PSNR, SSIM, and LPIPS metrics remain superior or comparable to each baseline, demonstrating that DC4GS enhances both compactness and reconstruction fidelity in 3DGS-based pipelines.

A.3.2 Additional qualitative comparisons

Fig. 9–11 provide additional qualitative comparisons between the baselines (Pixel-GS [44], 3DGS [14], and AbsGS [38]) and their DC4GS-integrated models.

Comparisons with Pixel-GS As shown in Fig. 9, DC4GS more effectively preserves linear boundaries, such as door panel patterns, counter edges, window frames, and lane markings. It also improves contrast in fine details and maintains distinct separation between adjacent regions, mitigating overshooting and bleeding artifacts.

Comparisons with 3DGS Fig. 10 shows that DC4GS improves the sharpness of architectural lines and geometric boundaries. It more accurately reconstructs fine structures like door panels, counter surfaces, window outlines, and wall trims. Straight edges and corners appear cleaner and less distorted, with reduced blending between adjacent objects and surfaces.

Comparisons with AbsGS In Fig. 11, DC4GS more reliably recovers structures such as window frames, rods, and wall seams, and reduces floating artifacts and blending at region boundaries (e.g., between sky, trees, and train). It suppresses redundant splits and improves local separation, resulting in clearer reconstructions with sharper object boundaries and fewer visual artifacts.

DC4GS consistently improves the reconstruction of fine structures and local detail, enhancing the separation between distinct objects and surfaces. This leads to reduced structural blending and clearer geometry in various scenes.

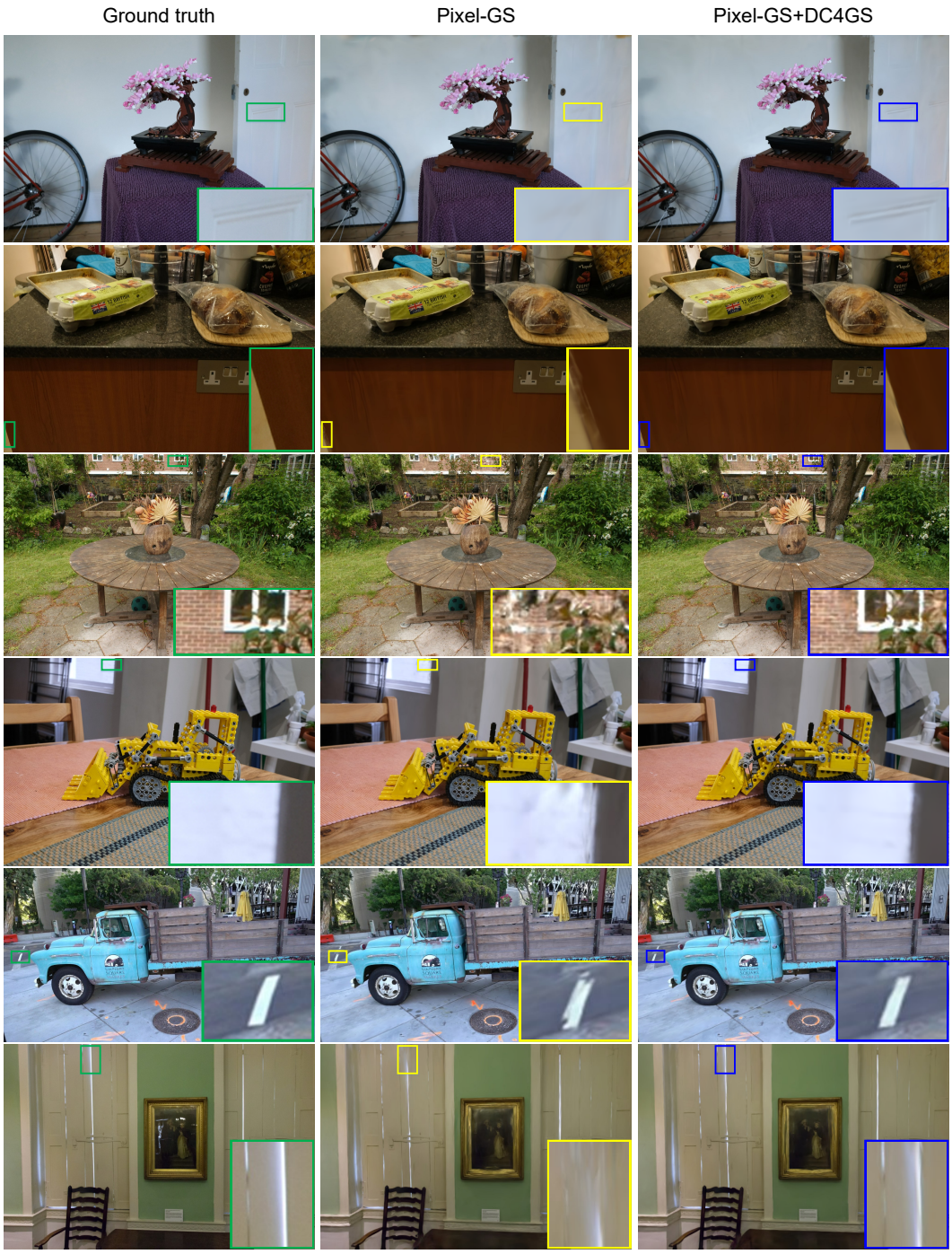

Figure 9: Qualitative visual comparisons between PixelGS and PixelGS integrated with DC4GS. The scenes, from top to bottom, are: Bonsai, Counter, Garden, Kitchen from the Mip-NeRF360 dataset, Truck from the Tanks&Temples dataset, and Dr Johnson from the Deep Blending dataset.

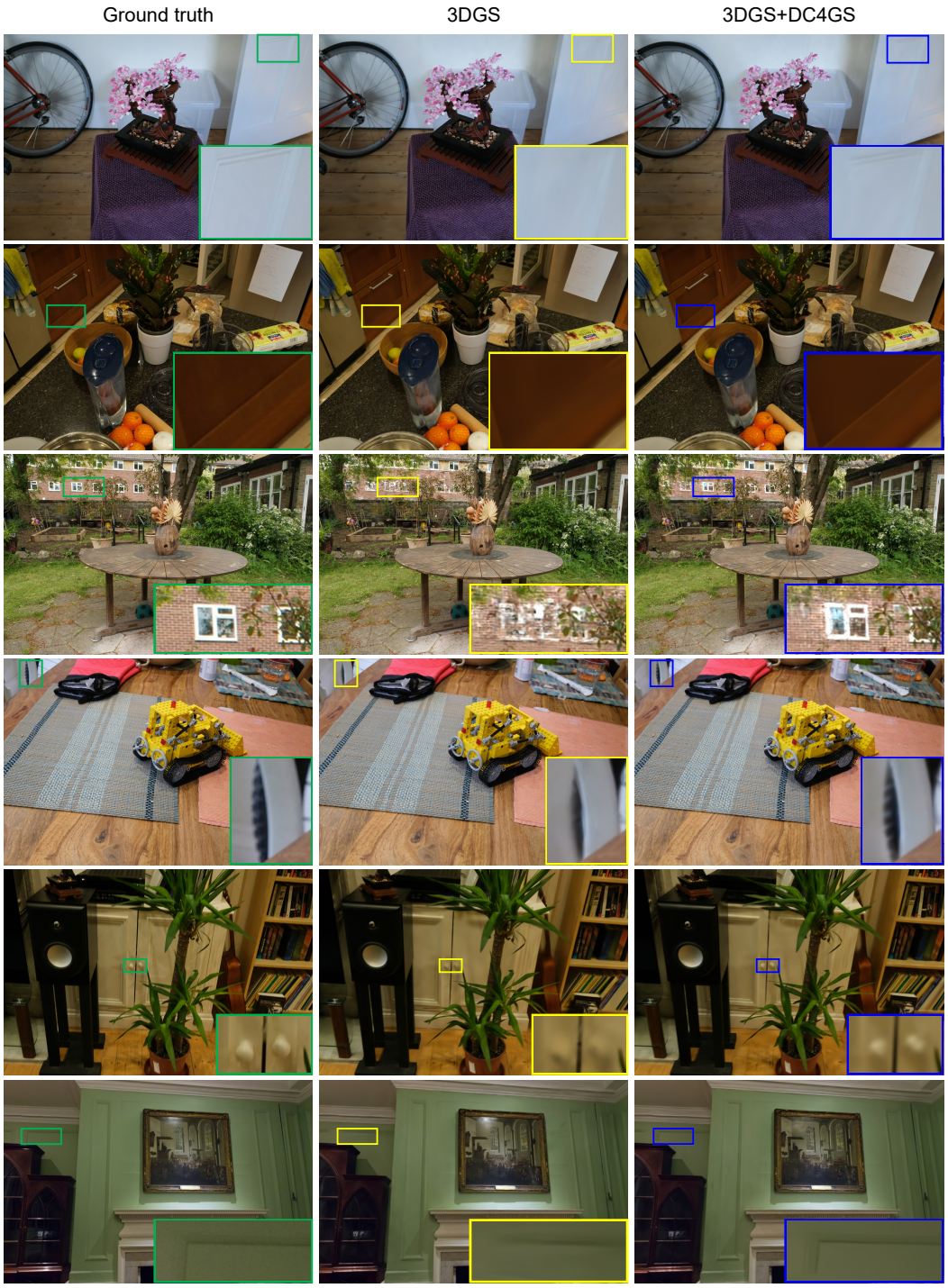

Figure 10: Qualitative visual comparisons between 3DGS and 3DGS integrated with DC4GS. The scenes, from top to bottom, are: Bonsai, Counter, Garden, Kitchen, Room from the Mip-NeRF360 dataset, and Dr Johnson from the Deep Blending dataset.

Figure 11: Qualitative visual comparisons between AbsGS and AbsGS integrated with DC4GS. The scenes, from top to bottom, are: Bicycle, Bonsai, Stump from the Mip-NeRF360 dataset, Train, Truck from the Tanks&Temples dataset, and Dr Johnson from the Deep Blending dataset.

Figure 12: Qualitative depth visualization comparison between AbsGS and AbsGS integrated with DC4GS. The scenes, from top to bottom, are: Bicycle from the Mip-NeRF360 dataset, and Truck from the Tanks&Temples dataset.

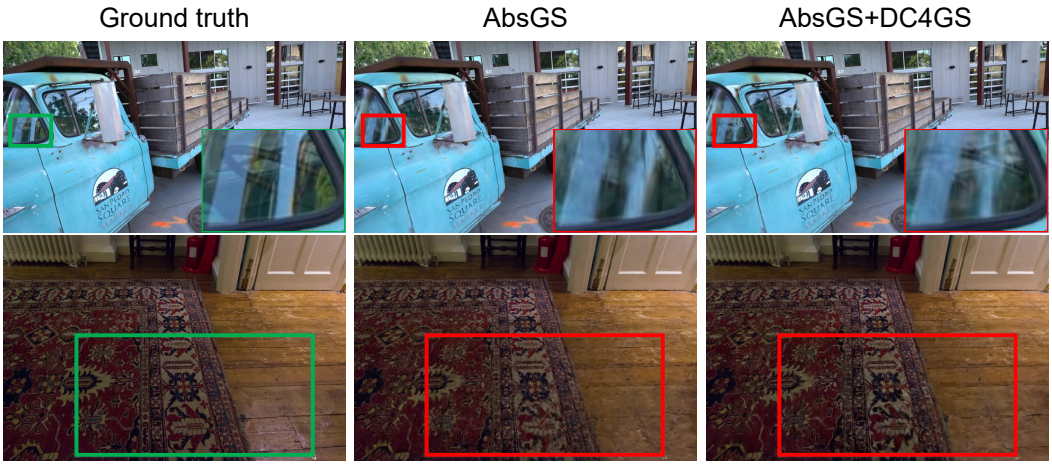

Figure 13: Qualitative comparisons on challenging cases between AbsGS and AbsGS integrated with DC4GS. The scenes, from top to bottom, are: Truck from the Tanks&Temples dataset (transparent objects), and Dr Johnson from the Deep Blending dataset (strong textures).

Table 8: Quantitative comparison between AbsGS and AbsGS integrated with DC4GS on challenging cases: transparency (Truck in Tanks&Temples) and strong textures (Dr. Johnson in Deep Blending).

Scene	Region	Method	PSNR ↑	SSIM ↑	LPIPS ↓
Truck	Transparent object	AbsGS	20.875	0.621	0.333
		AbsGS + DC4GS	**21.098**	**0.642**	**0.301**
Dr. Johnson	Strong texture	AbsGS	25.741	0.717	0.334
		AbsGS + DC4GS	**26.462**	**0.761**	**0.294**

A.3.3 Depth visualization comparison

We qualitatively assess geometric fidelity through depth map visualizations. To obtain depth maps, we adapt the original 3DGS rendering equation by replacing the RGB color contribution with per-Gaussian depth values d_i:

$$D = \sum_i T_i \cdot \alpha_i \cdot d_i, \quad T_i = \prod_{j=1}^{i-1}(1 - \alpha_j), \tag{4}$$

where α_i is the alpha and T_i is the transmittance value of the i-th Gaussian primitive.

As shown in Fig. 12, The baseline produces noisy depth maps. This noise mainly stems from the presence of numerous false-positive primitives that persist without proper density control. Such

Table 9: Quantitative comparison of 4DGS and 4DGS with DC4GS on D-NeRF and DyNeRF datasets, reporting quality metrics (PSNR, SSIM, LPIPS) and efficiency metrics (number of primitives, memory, training time, and rendering time in ms).

Dataset	Method	PSNR ↑	SSIM ↑	LPIPS ↓	Prim. ↓	Mem. ↓	Training ↓	Rendering ↓
D-NeRF [27]	4DGS [36]	34.063	**0.978**	**0.026**	45K	10MB	**9m**	15.233ms
	4DGS + DC4GS	**34.124**	**0.978**	**0.026**	**40K**	**9MB**	11m	**14.531ms**
DyNeRF [20]	4DGS	30.736	0.933	0.059	123K	59MB	**50m**	32.537ms
	4DGS + DC4GS	**31.092**	**0.936**	**0.056**	**119K**	**56MB**	1h 13m	**32.259ms**

primitives contribute spurious depth values, leading to fragmented and unstable geometry. In contrast, DC4GS effectively suppresses false-positive primitives, yielding cleaner and more coherent depth reconstructions. This suggests that the benefits of DC4GS extend beyond RGB fidelity to improved structural consistency.

A.3.4 Applicability to challenging scenarios

To evaluate DC4GS under challenging conditions, we perform region-specific comparisons on transparency and strong textures. Quantitative results, measured on the masked inset regions in Fig. 13, are reported in Table 8, and the corresponding qualitative comparisons are also shown in Fig. 13.

For the transparent objects (4th test image of the Truck scene in Tanks & Temples), the baseline fails to reconstruct the internal features behind the glass (e.g., steering wheel), whereas DC4GS successfully preserves these structures. For strong high-frequency textures (9th test image of the Dr. Johnson scene in Deep Blending), such as carpet patterns and wood scratches, DC4GS achieves superior metrics over the baseline, showing its ability to capture fine details. These results suggest that DC4GS can better handle transparent and high-frequency regions that are challenging for the baseline.

A.3.5 Applicability to dynamic scenes

We further evaluate DC4GS on dynamic scenes by integrating it into 4DGS [36] and testing on D-NeRF [27] and DyNeRF [20]. As shown in Table 9, DC4GS yields consistent improvements in reconstruction quality, while reducing the number of primitives and memory usage, which also leads to faster rendering. Qualitative comparisons in Fig. 14 show that DC4GS produces sharper geometry and more temporally stable appearance, whereas 4DGS often exhibits blurred details and temporal artifacts. Despite the increased training time, these results suggest that DC4GS remains effective and robust in dynamic scenarios.

A.4 Limitations and future work

DC4GS enables high-quality reconstruction with substantially fewer primitives, resulting in faster rendering and reduced memory consumption for 3DGS models. Although the method introduces additional training overhead due to directional consistency evaluation and candidate split cost estimation, this overhead is confined to the training phase and can be entirely removed once the densification stage is complete (typically after 15,000 iterations). Future work will focus on optimizing the DC computation and split estimation pipeline, particularly the cost evaluation and polynomial regression, to further reduce training time without compromising reconstruction quality.

A.5 Broader impact

DC4GS improves the efficiency of 3DGS by reducing primitive count without compromising quality. This leads to lower memory usage for 3DGS parameters and faster rendering, making high-quality 3D reconstruction more accessible for real-time and resource-constrained applications such as AR/VR and mobile platforms.

As with other 3D reconstruction techniques, there is potential for misuse (e.g., unauthorized duplication of real-world scenes). Responsible use and ethical considerations remain important in downstream applications.

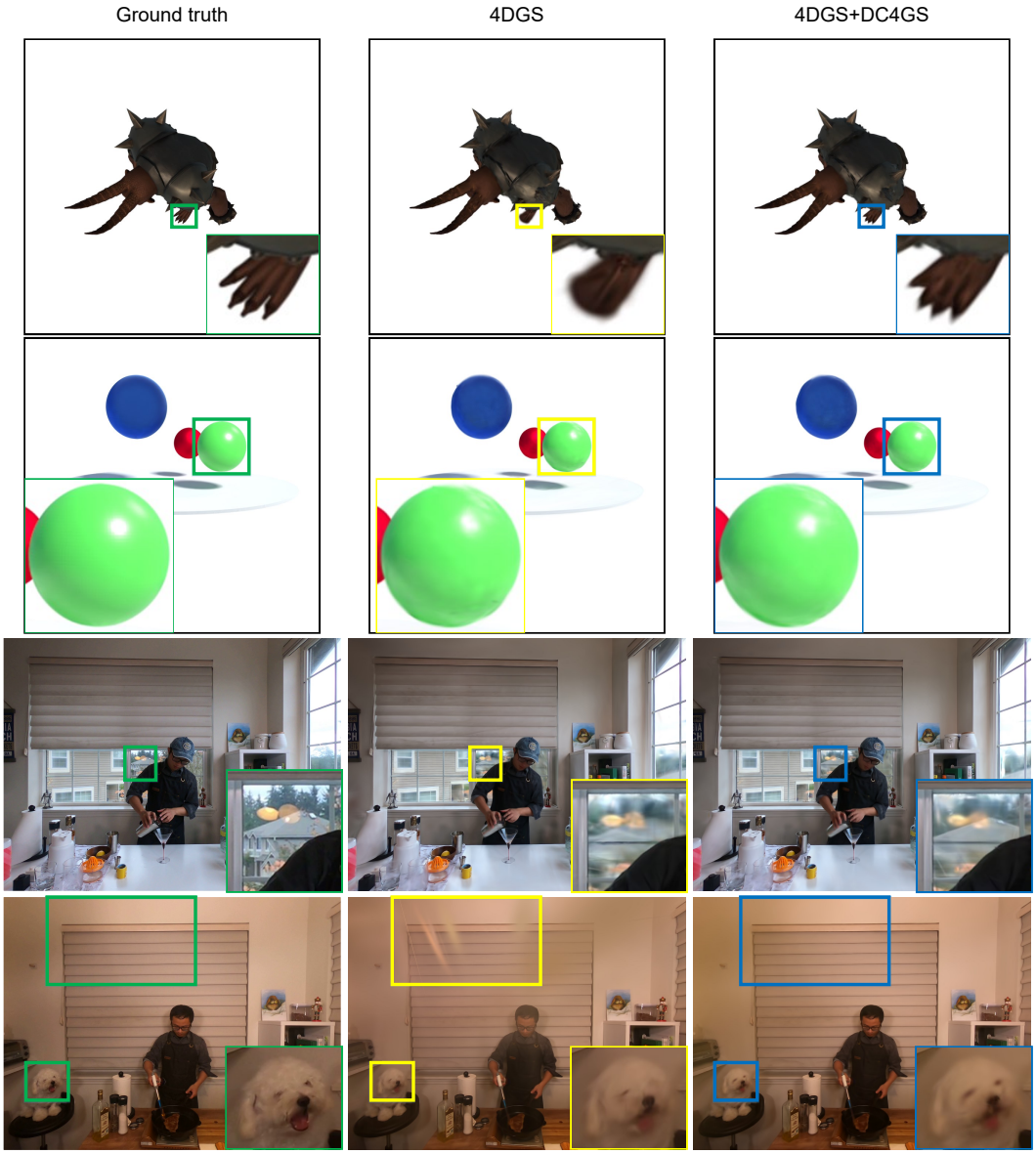

Figure 14: Qualitative comparisons on dynamic scenes between 4DGS and 4DGS with DC4GS. The scenes, from top to bottom, are: Bouncing balls and Hell warrior from the D-NeRF dataset, and Coffee martini and Flame steak from the DyNeRF dataset.

A.6 Dataset licenses

We use the following datasets in our experiments:

- Mip-NeRF360 [2]: no explicit license terms provided. Available at https://jonbarron.info/mipnerf360/.
- Tanks and Temples [16]: released under the Creative Commons Attribution 4.0 International (CC BY 4.0). Available at https://www.tanksandtemples.org/license/.
- Deep Blending [12]: no explicit license terms provided. Available at http://visual.cs.ucl.ac.uk/pubs/deepblending/.